

Evolution of Cell Shape in Bacteria

A thesis submitted in partial fulfilment of the requirements for the
BS-MS Dual Degree Programme

By:
Malavika Venu
20151054

May, 2020

Department of Biology
Indian Institute of Science Education and Research
Dr Homi Bhabha Road
Pashan, Pune 411008
India



With guidance from,
Dr David W. Rogers

Supervised by:
Dr Paul B. Rainey

Max Planck Institute of Evolutionary Biology
August Theinemann Street 2
24306 Plön, Schleswig Holstein
Germany



Max-Planck Institut für
Evolutionsbiologie, Plön

© Malavika Venu 2020

All rights reserved

CERTIFICATE

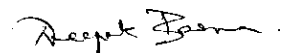
This is to certify that this dissertation entitled “Evolution of Cell Shape in Bacteria” towards the partial fulfilment of the BS-MS dual degree program at the Indian Institute of Science Education and Research, Pune represents work carried out by Malavika Venu at the Max Planck Institute of Evolutionary Biology, Plön under the supervision of Dr Paul B. Rainey, Director, Department of Microbial Population Biology, Max Planck Institute of Evolutionary Biology, Plön during the academic year 2019-2020.



Malavika Venu
20151054
5th year BS-MS
IISER, Pune

Committee:

Expert advisor:



Dr Deepak Barua
Associate Professor
IISER
Pune

Supervisor:



Dr Paul B. Rainey
Director
MPI for Evolutionary Biology
Plön

DECLARATION

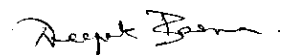
I hereby declare that the matter embodied in the report entitled “Evolution of Cell Shape in Bacteria” are the results of the work carried out by me at the Department of Microbial Population Biology, Max Planck Institute of Evolutionary Biology, Plön, under the supervision of Dr Paul B. Rainey and the same has not been submitted elsewhere for any other degree.



Malavika Venu
20151054
5th year BS-MS
IISER, Pune

Committee:

Expert advisor:



Dr Deepak Barua
Associate Professor
IISER
Pune

Supervisor:



Dr Paul B. Rainey
Director
MPI for Evolutionary Biology
Plön

ABSTRACT

In this study we attempted to understand the evolution of bacterial cell shape, by investigating the function of different proteins involved in cell shape and division in the rod-shaped bacteria *Pseudomonas fluorescens*, SBW25. This was primarily in the context of the unfit, spherical, asymmetrically dividing $\Delta mreB$ mutants of SBW25, that evolved to increase fitness and divide symmetrically after being subjected to a long-term evolution experiment. Firstly, we found that the compensatory point mutation that arose in *pbp1A* gene in these mutants, speculated to cause loss of function was different from the *pbp1A* deletion mutant in the wildtype background and hence might have an altered function. Secondly, we identified the protein MinC in SBW25, found that it localises to one of the poles of the cell and its inactivation gave rise to cells that had decreased fitness and serious cell division defects dependent on the environment. The study has led to an improvement in bacterial selection techniques, microscopy and bacterial cell morphology quantitation. By providing better understanding about *pbp1A* and *minC* in wildtype cells and improved techniques, the study has opened up the possibility to understand their implications in the fitness and symmetry of division in the evolved and ancestral $\Delta mreB$ mutants and has given $\Delta minC$ mutant as the next candidate for a long-term evolution experiment.

TABLE OF CONTENTS

1. CERTIFICATE.....	2
2. DECLARATION.....	3
3. ABSTRACT.....	4
4. LIST OF FIGURES.....	6
5. LIST OF TABLES.....	7
6. ACKNOWLEDGEMENTS.....	8
7. INTRODUCTION.....	9
8. RESULTS.....	14
i) Deletion of <i>pbp1A</i> in <i>P. fluorescens</i> SBW25	
ii) Characterisation of <i>pbp1A</i> mutants	
iii) Deletion of <i>minC</i> in <i>P. fluorescens</i> SBW25	
iv) Genome sequencing of Δ <i>minC</i> SBW25 showed the absence of compensatory mutations	
v) Characterisation of <i>minC</i> mutants	
vi) GFP tagged <i>minC</i> was constructed in <i>P. fluorescens</i> SBW25	
vii) Endogenous msfGFP tagged MinC gave a weak signal	
viii) Inducible msfGFP-MinC plasmid was constructed	
ix) Expression of msfGFP-MinC via plasmid generates elongate green cells	
x) Tn-7 inducible fluorescent tagged <i>minC</i> in wildtype and Δ <i>minC</i> strains were constructed	
xi) Tn-7 inducible msfGFP-MinC localised to the poles/ prospective poles in WT and Δ <i>minC</i> cells respectively	
9. DISCUSSION.....	37
10. MATERIALS AND METHODS.....	43
11. REFERENCES.....	60

LIST OF FIGURES:

Figure 1: Rod shape of bacilloid cells is maintained by the elongasome

Figure 2: Phylogenetic tree showing presence of MreB

Figure 3: MinCD system

Figure 4: Deletion of *pbp1A*

Figure 5: Characterisation of *pbp1A* mutants

Figure 6: Relative fitness of *pbp1A* mutants

Figure 7: Deletion of *minC*

Figure 8: Genome sequencing results of $\Delta minC$ mutant

Figure 9: *minC* mutants visualised in LB

Figure 10: Characteristic comparison of *minC* mutants in LB and M9

Figure 11: Quantitative comparison of *minC* mutants in LB and M9

Figure 12: Relative fitness of *minC* mutants

Figure 13: Construction of msfGFP-MinC mutant

Figure 14: Characterisation of msfGFP-MinC mutant

Figure 15: Construction of pSCM cyclohexanone inducible msfGFP-MinC mutant

Figure 16: Characterisation of pSCM cyclohexanone inducible msfGFP-MinC mutant

Figure 17: Construction of Tn7cyclohexanone inducible msfGFP-MinC mutant

Figure 18: Characterisation of Tn7cyclohexanone inducible msfGFP-MinC mutant

Figure 19: Two step allelic exchange

Figure 20: Workflow of *pbp1A* mutant cell measurements

Figure 21: Workflow of $\Delta minC$ cell measurements

LIST OF TABLES:

Table 1: Antibiotics and supplements used in this study

Table 2: *P. fluorescens* strains used in this study

Table 3: *E. coli* strains used in this study

Table 4: Plasmid vectors used in this study

Table 5: Primers used in this study

Table 6: Components used for normal PCR

Table 7: Reaction conditions for normal PCR

Table 8: Components used for colony PCR

Table 9: Reaction conditions for colony PCR

Table 10: Components used for Sanger sequencing

Table 11: Reaction conditions used for Sanger sequencing

ACKNOWLEDGEMENTS

I am grateful to Dr Paul B. Rainey, my supervisor for giving me this incredible opportunity to work in his research group at the Max Planck Institute of Evolutionary Biology, Plön and exposing me to a group of amazing scientists. I am forever indebted to Dr David W. Rogers, for being patient with me, answering all my questions, guiding me over the course of this project, making this manuscript readable and motivating me to be the best version of myself. It is his contagious enthusiasm that helped me surpass the obstacles faced in this project. I sincerely thank Dr. Deepak Barua, my advisor for valuable inputs and support he provided throughout the project. I would also like to thank Dr Jana Grote for her assistance in microscopy, Dr Tatyana Pichugina and Dr Nikola Ojkic for providing the automated cell measurement program service, Dr Javier López-Garrido and Dr Clara Moreno-Fenoll for their valuable suggestions that considerably improved my microscopy skills. I extend my appreciation to all members of the Microbial Population Biology department, who made my work environment absolutely pleasurable. Last, but not the least I express my sincere gratitude to my family and friends, for their encouragement and constant support. Thank you for believing in me.

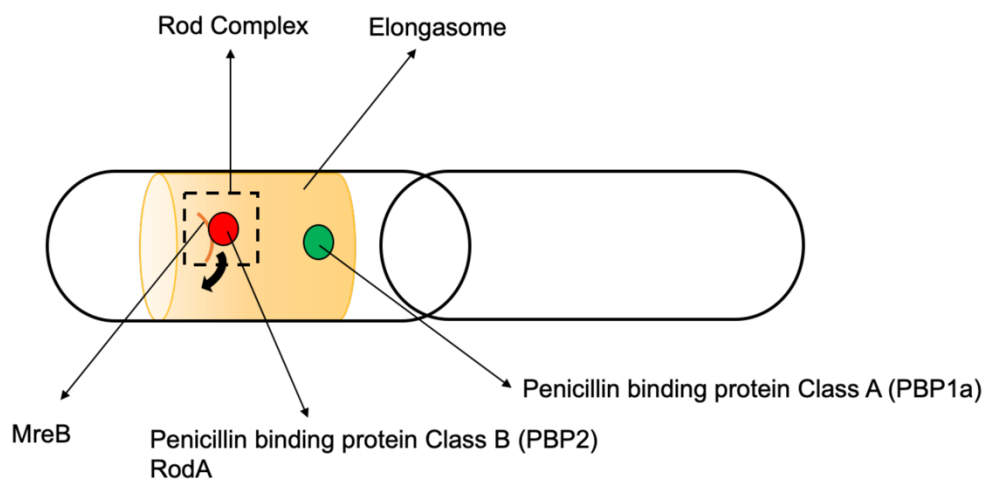
INTRODUCTION

Bacteria exhibit a multitude of cell morphologies. The wide diversity of bacterial cell shapes one observes in nature is suggestive of the adaptive value the trait encompasses. Each cell shape confers specific advantages under different environmental conditions resulting in natural selection and the consequent evolution of the trait (Young, 2006). Two simple bacterial cell shapes of interest to this project are coccoid and bacilloid, which can be thought of as two shapes present at the extremes of the cell shape spectrum. Rod-shaped bacteria thrive in nutrient-rich environments, while spherical shaped bacteria grow better in nutrient-depleted, fluctuating environmental conditions. The primary reason for this is the higher surface area to volume ratio offered by the rod shape as opposed to the spherical shape, which has the lowest surface area to volume ratio (Watve, 1997). Coccoid shape is an evolutionary dead-end, unable to evolve to any other shape and has evolved multiple times, independently from bacilloid and filamentous forms of bacteria, as shown by phylogenetic evidence (Young, 2006). The ease with which rod-shaped bacteria can convert to spherical shape, usually by targeting a key cell shape-determining gene via antibiotics (Monahan et al., 2014; Ogura et al., 1989) or deletion (Shiomi et al., 2008; Wachi et al., 1987; Yulo et al., 2018) also reaffirms this observation. This is contrary to the belief that they were the first cells and the progenitor of the different cell shapes that exist today (Young, 2006). Therefore, looking in to the molecular underpinnings of cell shape in bacteria and identifying key differences between coccoid and bacilloid bacteria, will prove helpful in understanding the how the evolutionary transition from bacilloid to coccoid shape could have happened.

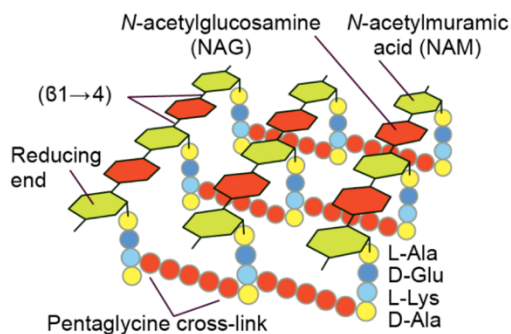
Bacterial cell shape is mainly determined by peptidoglycan, the primary structural component of the cell wall. Two types of cell machinery take part in the incorporation of peptidoglycan into the cell wall. One is the divisome, present in all bacteria, responsible for the formation of the division septa, which splits the cell into two (Pinho et al., 2013) and the other is the elongasome, which as the name suggests is, responsible for the longitudinal elongation of the cell, prior to cell division and is present only in rod-shaped bacteria (van Teeffelen and Renner, 2018). Hence the loss of elongasome seems to be a plausible step that could have facilitated the transition from rod-shaped cells to spherical cells.

The elongasome consists of the rod complex and the bifunctional Penicillin-Binding Protein 1 class A (PBP1a), which has both transpeptidase and transglycosylase properties. The rod complex consists of monofunctional transpeptidase Penicillin-Binding Protein 2 class B (PBP2) and the transglycosylase Rod A and Rod Z that attach to the bacterial equivalent of actin - MreB protein. Transglycosylation is the elongation of the peptidoglycan chain by joining peptidoglycan molecules together, while transpeptidation is the peptide crosslinking of two glycan chains. Both these processes are required for the polymerization of peptidoglycan (Fig.1).

A.



B.



C.

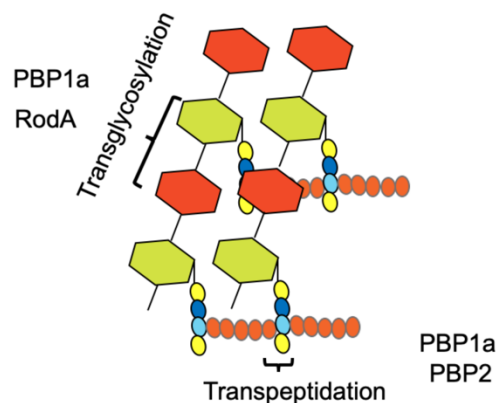


Fig. 1: Rod shape of bacilloid cells is maintained by the elongasome.

Schematic of the A) elongasome B) peptidoglycan and C) processes carried out in peptidoglycan synthesis by the members of elongasome.

It is speculated that rod complex is involved in the systematic incorporation of peptidoglycan into the cell wall, while PBP1a moves around more or less randomly, focusing on confined cell wall areas for the same (Cho et al., 2016). Based on previous

studies conducted on the members of the rod complex (Veyrier et al., 2015) and the evident absence of *mreB* in many coccoid bacteria (Fig. 2) (Pinho et al., 2013), Yulo and colleagues (Yulo et al., 2018) deleted *mreB* in *Pseudomonas fluorescens*, SBW25, generating spherical cells. However, this came with a considerable cost to the cells. They found that the bacteria divided asymmetrically, often producing non-viable cells without DNA. They then went on to do a long-term evolution experiment with these mutant cells, spanning 1000 generations. Long-term evolution experiments were pioneered by Richard Lenski (Lenski, 2017; Lenski et al., 1991) to study the mutations that spread in the long run in *Escherichia coli* replicate populations. Yulo and colleagues (Yulo et al., 2018) used this technique as a powerful tool to evolve compensatory mutations that arose as a consequence of the gene deletion.

Over the course of 1000 generations, evolved bacteria remained spherical, with higher fitness than the non-evolved $\Delta mreB$ mutants. Symmetric division was also restored. Point mutations in *pbp1a* were found to be one of the compensatory mutations leading to enhanced fitness in these mutants. The compensatory mutations in *pbp1a* that arose in $\Delta mreB$ mutants, when recreated in wildtype, have negligible effects on growth, but the cells were thinner than the ancestor. Four independent point mutations in *pbp1a* were identified to compensate for MreB loss in SBW25. One of the point mutations is close to the transpeptidation active site of PBP1a. A similar mutation has been shown to cause decreased reactivity of PBP1a to β -lactams in *Streptococcus pneumoniae* (Job et al., 2008). Similar to the case of MreB, coccoid cells generally have a significantly lower number of PBPs compared to bacilloid bacteria. Based on these observations, they (Yulo et al., 2018) speculated that the compensatory mutation led to loss of function of the PBP1a.

The large fitness cost of deleting *mreB* can be attributed to the inability of mutants to divide symmetrically; many of their progeny are minicells that lack nuclei entirely and therefore cannot reproduce. Symmetric division was found to be restored after

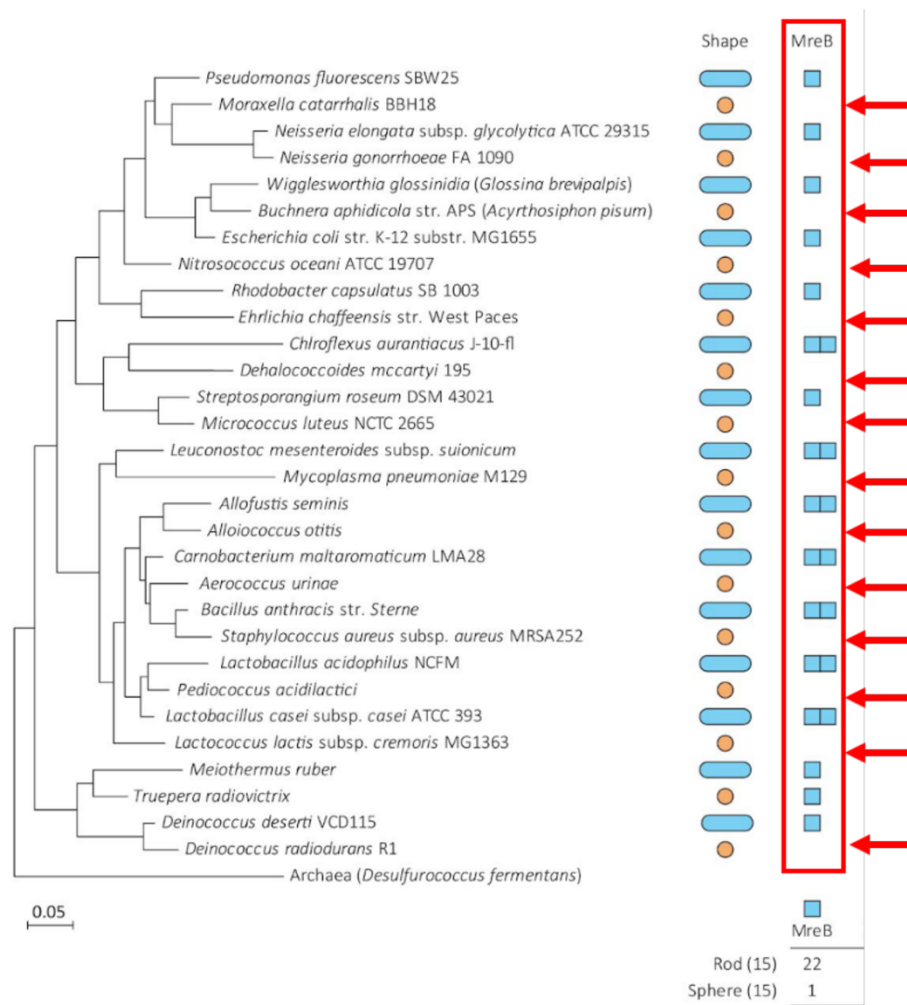


Fig. 2: MreB is not present in many coccoid bacteria. Adapted from Yulo et al., 2018

evolution. What leads to the asymmetric division in these cells and retrieval of symmetric division after evolution? Various proteins have been implicated in the regulation of cell division in bacteria (Pinho et al., 2013). In *E. coli*, symmetric cell division is facilitated by the MinCDE system, which consists of MinC, MinD and MinE proteins. MinD is an adenosine triphosphatase (ATPase) that binds to the cell membrane. When MinD is bound to ATP (MinD-ATP), it can engage MinC, which inhibits the formation of the Z-ring, that divides the cell. This assembly grows along the cell membrane to mid-cell, where MinE is present and forms a ring-like structure that moves towards the pole hydrolysing MinD-ATP to MinD-ADP, which results in its loss of affinity to the cell membrane. MinD-ADP then moves to the opposite pole where the concentration of MinE is lowest, getting converted to MinD-ATP on the way and

attaching to the membrane and binding MinC again. The process repeats, which results in the pole to pole oscillation of MinC, polarising the cell and establishing division in the middle of the cell, where the average concentration of MinC is the lowest. (Fig. 3) (Veiga and Pinho, 2012). Oscillations may not always be essential for specification of the division site. For instance, *Bacillus subtilis* exhibits an immobile gradient of MinC and MinD from the cell poles to the centre. The organism lacks MinE, and it has been speculated that the protein DivIVA localises to the cell poles and later recruits MinC and MinD. However, the exact mechanism of cell division regulation by these proteins is not well understood (Lutkenhaus, 2007).

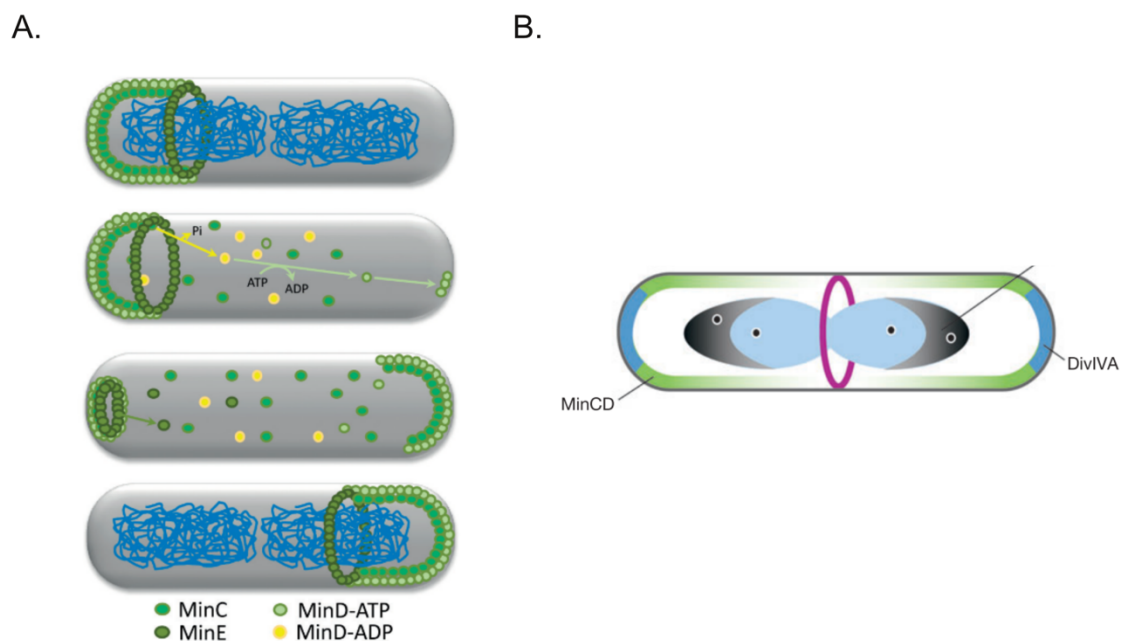


Fig. 3: MinCD systems in *E. coli* and *B. subtilis*. A) MinCD oscillates from pole to pole in *E. coli* (Image adapted from Veiga and Pinho, 2012) B) MinCD is static and present at both the poles in *B. subtilis* (Image adapted from Lutkenhaus 2017).

How vital is MinC for the proper division of the cell? Removal of MinC has been shown to result in the formation of minicells in *E. coli* (de Boer et al., 1991) and delay in cell division of *B. subtilis* (Rodrigues and Harry, 2012). In *Neisseria gonorrhoea*, the deletion led to an increase in size and lysis of the cells (Ramirez-Arcos et al., 2001), while in *Agrobacterium tumefaciens*, no visible phenotype was observed (Flores et al.,

2018). The *minC* deletion mutants of *P. aeruginosa* were shown to be viable with a minicell phenotype (Carter et al., 2017) although in a recent study, MinC was shown to be essential in rich media for *P. aeruginosa*, but not in minimal media (Poulsen et al., 2019). Insertions in the *minC* have not been reported in any of the genome-wide Tn5 insertional mutagenesis libraries created for three different strains of *P. fluorescens* (see supplementary table 20 in (Price et al., 2018)), consistent with the observation that MinC might be essential in *Pseudomonas* - although it remains possible that these particular insertions failed to occur in any of the libraries .

Based on the observations and questions raised above, this project attempts to do the following in the model organism *P. fluorescens* SBW25:

- Check if the compensatory point mutations in *pbp1a* that arose in the Δ *mr**reB* mutants are consistent with a complete loss of PBP1a function. Nonsense and frame-shift mutations are often a reliable way to cause loss of function of a gene. Absence of such mutations in *pbp1a* and occurrence of point mutations instead, suggests that the compensatory mutations might alter the function of PBP1a rather than eliminating it entirely. Hence, we deleted *pbp1A* from the SBW25 genome and compared the fitness and cellular morphology of the Δ *pbp1A* mutant with those of an evolved point mutant and the wildtype.
- MinC has been implicated in the symmetric division of bacilloid cells. Sequence-based homology shows that *P. fluorescens* SBW25 has the MinC homologue. However, we don't know what role, if any, the protein plays in cell division in wildtype *P. fluorescens*, let alone how this system functions in spherical Δ *mr**reB* cells. Is it similar to *E. coli* or *B. subtilis* or is it via a novel mechanism? To answer this, we attempted to fluorescent tag MinC protein in *P. fluorescens* SBW25 wildtype cells and observe the dynamics of the protein in the cell. Owing to the diverse consequences of *minC* deletion across bacterial species and evident disparity in conclusions from previous studies involving *Pseudomonas*, we attempted to check if the deletion of *minC* was viable in *P. fluorescens* SBW25 and if yes, characterise the consequent phenotype and fitness.

RESULTS

Deletion of *pbp1A* in *P. fluorescens* SBW25

The *pbp1a* gene had compensatory mutations in multiple evolved $\Delta mreB$ lineages. Most of these were point mutations, including the single nucleotide transition G1450A. Due to the location of this mutation, Yulo and colleagues (Yulo et al., 2018) speculated it to be a loss of function mutation. However, nonsense and frame-shift mutations were not observed. To test if the point mutation leads to loss of function, *pbp1a* and a closely located repeat region on the 5' end of the gene was deleted from the SBW25 genome (See methods). Repeat sequences have palindromes that interfere with the efficient sequencing of the construct. To confirm the deletion, we screened colonies obtained after cycloserine enrichment using colony PCR with two primers that flanked the region to be deleted (Fig. 4A). An unsuccessful deletion will give a 3.2 kb product (Fig. 4A) while a successful deletion will give a 682 bp product (Fig. 4B). Agarose gel electrophoresis showed that the amplified fragment was consistent with the smaller size (Fig. 4C). Sanger sequencing of the obtained product confirmed the deletion.

Characterisation of *pbp1A* mutants:

The point mutation G1450A in *pbp1A* gene in the evolved $\Delta mreB$ mutant was recreated in the wildtype (WT) by Yulo and colleagues. The mutation had no prominent fitness effect, but the cells were found to be thinner than in the wildtype. To determine if the deletion mutant has a similar or different phenotype and fitness, we went on to characterise and compare the WT, *pbp1A* (G1450A) and $\Delta pbp1A$ strains in terms of phenotype and fitness.

a) *pbp1A* deletion mutant has different cell morphology than the point mutant

To test the phenotypic consequences of *pbp1A* deletion and compare it with the point mutant of *pbp1A*, we visualised WT (Fig. 5A), *pbp1A* (G1450A) (Fig. 5B), $\Delta pbp1A$ (Fig. 5C) cells under the microscope. Membrane dye (FMTM4-64) staining (see methods) was used to get sharp contours, to increase the accuracy of the measurements. Cell morphology parameters including length (Fig. 5D), width (Fig. 5E), and area (Fig. 5F) of the WT, *pbp1A* (G1450A) and $\Delta pbp1A$ were measured using the Cell Segmentation program developed by Tatyana Pichugina (see methods) and compared. In terms of length of the cell,

both the *pbp1A* (G1450A) ($2.02 \pm 0.01 \mu\text{m}$) and Δ *pbp1A* ($1.97 \pm 0.02 \mu\text{m}$) mutants were shorter than the wildtype ($2.23 \pm 0.02 \mu\text{m}$) (Fig. 5D). In terms of width and area of the cell, all the three strains differed from each other. Wildtype strain had the greatest width and area ($1.070 \pm 0.003 \mu\text{m}$ and $1.81 \pm 0.02 \mu\text{m}^2$ respectively), followed by Δ *pbp1A* ($1.059 \pm 0.003 \mu\text{m}$ and $1.59 \pm 0.01 \mu\text{m}^2$ respectively) and *pbp1A* (G1450A) ($0.990 \pm 0.002 \mu\text{m}$ and $1.50 \pm 0.01 \mu\text{m}^2$ respectively) (Fig. 5D and 5E). Analysis of variance (ANOVA) performed on each measurement showed that differences between strains were greater than expected by chance for the length, width and area of the cell (Fig 5DEF) and pairwise differences between groups were identified using Tukey HSD tests.

b) Mutations in *pbp1A* did not affect fitness

In order to check for fitness effects of the point and deletion mutants, we tagged the wildtype, *pbp1A* (G1450A) and Δ *pbp1A* mutants with Green Fluorescent Protein (GFP) and Red Fluorescent Protein (RFP) separately. Fluorescent tagging was so that we could measure the number of cells of each kind using fluorescent flow cytometry. To ensure that the different fluorophores did not have different effects on fitness we competed each GFP tagged strain of WT, *pbp1A* (G1450A) and Δ *pbp1A* against the RFP tagged versions of the same strain and measured the relative fitness. The relative fitness of the GFP and RFP tagged strains were all very close to 1, indicating no difference in the fitness costs of the markers (Fig. 6). We then went on to compete *pbp1A* (G1450A)-RFP against the WT-GFP, Δ *pbp1A*-RFP against the wildtype GFP and *pbp1A* (G1450A)-RFP against Δ *pbp1A*-GFP and vice versa. Differences observed between strains were not greater than would be expected by chance ($P=0.9694$) indicating that all strains had similar fitness.

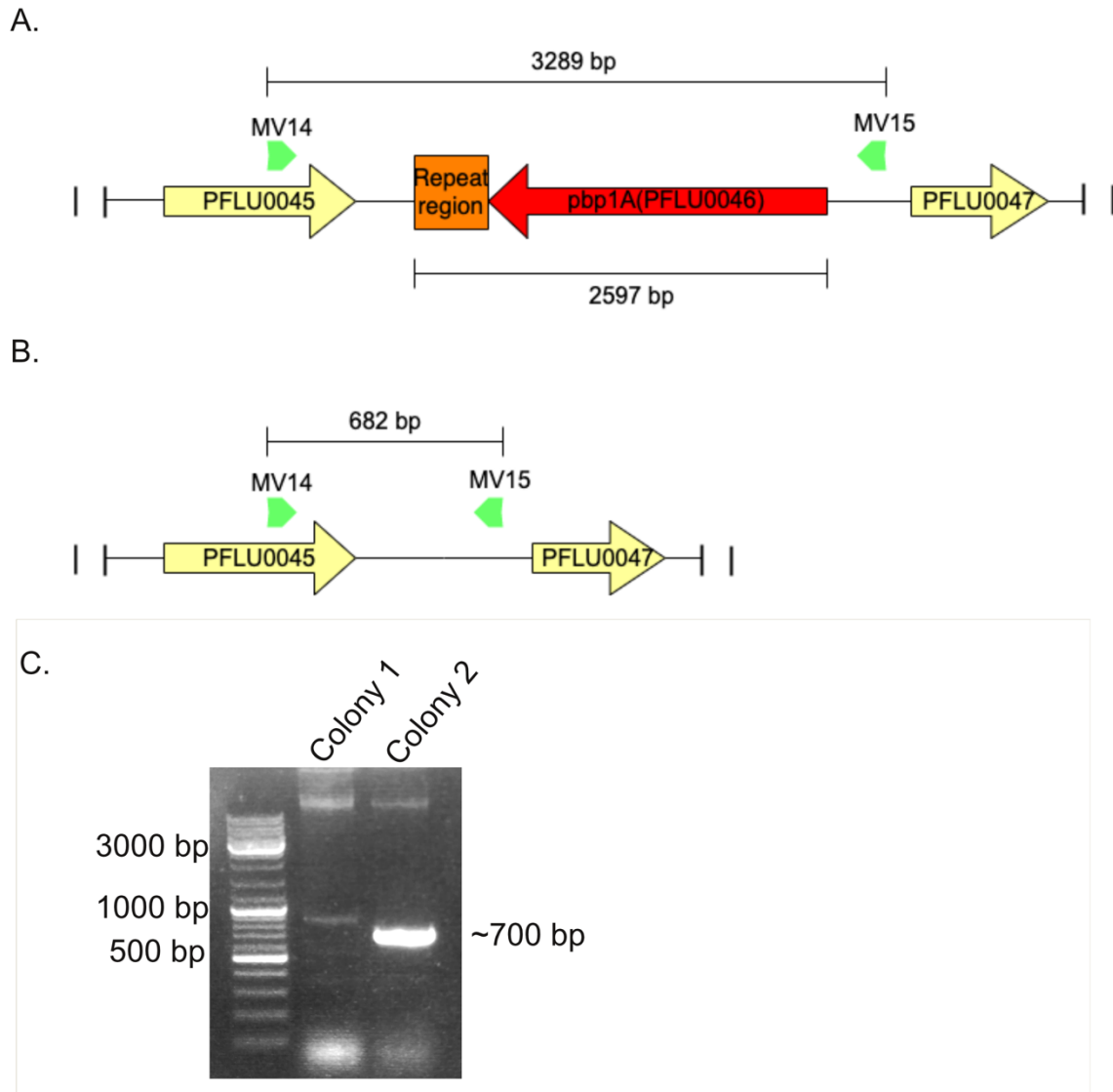


Fig. 4: *pbp1A* was deleted from the SBW25 genome. A) Representative image showing the size and location of the region to be deleted, along with the primers used to confirm the deletion. B) Expected product size, if the deletion is successful. C) Colony-PCR gel image showing the confirmation of deletion.

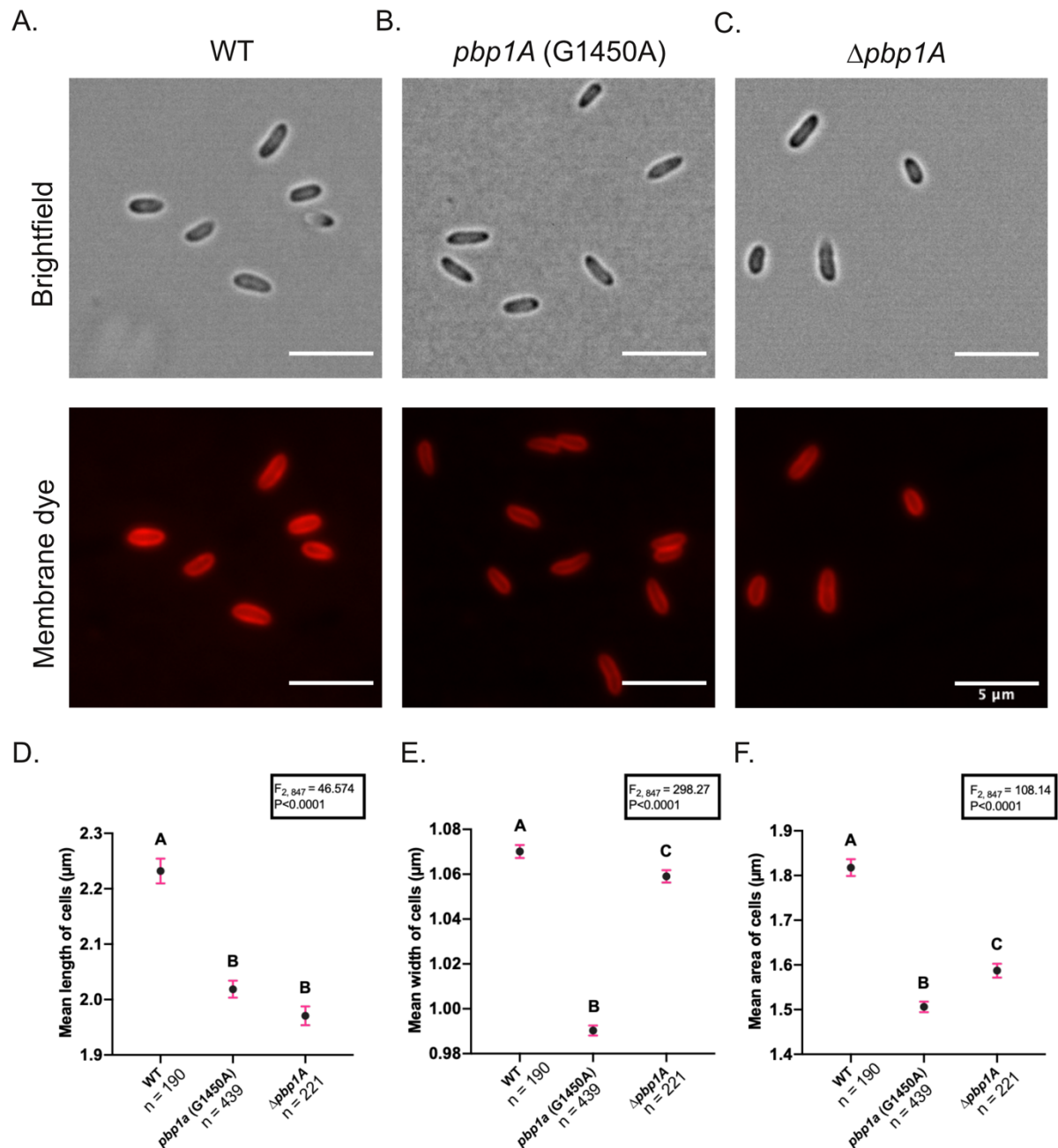


Fig. 5: *pbp1A* (G1450A) differs from $\Delta pbp1A$ in terms of width and area, but not length of the cell. Brightfield and membrane stained(FMTM4-64) images of A) WT, B) *pbp1A* (G1450A) C) $\Delta pbp1A$ strains grown on LB. Scale bar = 5 μ m. Measurements of mean cell D) length E) width and F) area. One biological replicate was measured. Number of cells (n) measured as indicated. Error bars represent SEM. F-statistic for the parameters explaining the variance as depicted. Within each parameter, measures not indicated by the same letter are significantly different as per the Tukey HSD test. $P < 0.05$.

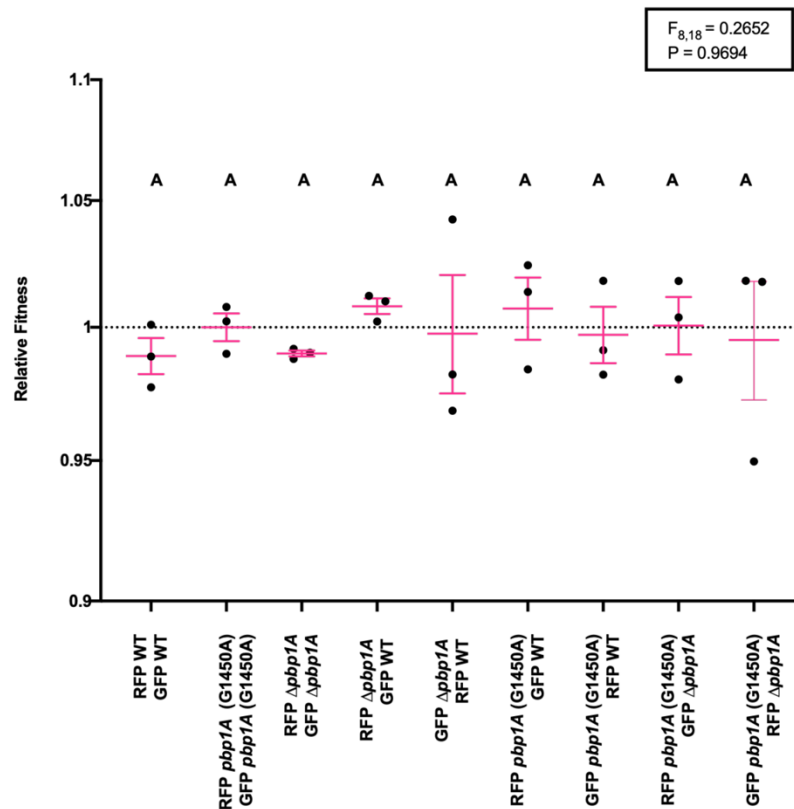


Fig. 6: Differences in relative fitness between the Wildtype, *pbp1A* (G1450A) and Δ *pbp1A* strains were not greater than observed by chance. A) Relative fitness measures of the RFP tagged strain against the GFP tagged strains of Wildtype, *pbp1A* (G1450) and Δ *pbp1A* SBW25 against each other, *pbp1A* (G1450A) against Wildtype, Δ *pbp1A* against Wildtype and *pbp1A* (G1450A) against Δ *pbp1A*. Three biological replicates were used. Error bars represent SEM. F-statistic represents the failure of strain competition combinations to explain more of the variance in relative fitness than expected by chance. Measures indicated by the same letter indicates the failure to detect significant difference.

Deletion of *minC* in *P. fluorescens* SBW25

Δ *mreB* mutants were unable to divide symmetrically initially and later evolved to divide symmetrically. Normal rod-shaped bacteria divide symmetrically either by oscillations of the MinCDE or an immobile gradient of MinCD along the longitudinal axis of the cell. Deletion of MinC has varied effect over different bacterial species which includes the formation of minicells, lysis of cells and delay in cell division. Mechanics of how MinC behaves in *P. fluorescens* is unknown. To get a better understanding about the gene and its function in SBW25, we deleted the gene *minC* from the SBW25 genome. Colonies obtained after cycloserine enrichment were screened using colony PCR with

two primers that flanked the region to be deleted (Fig. 7A), to confirm the deletion. An unsuccessful deletion will give a 2.5 kb product (Fig. 7A) while a successful deletion will give a 1.8kb product (Fig. 7B). The amplified fragment was around 2kb, as per agarose gel electrophoresis results (Fig. 7C). The deletion was confirmed by Sanger sequencing the obtained product.

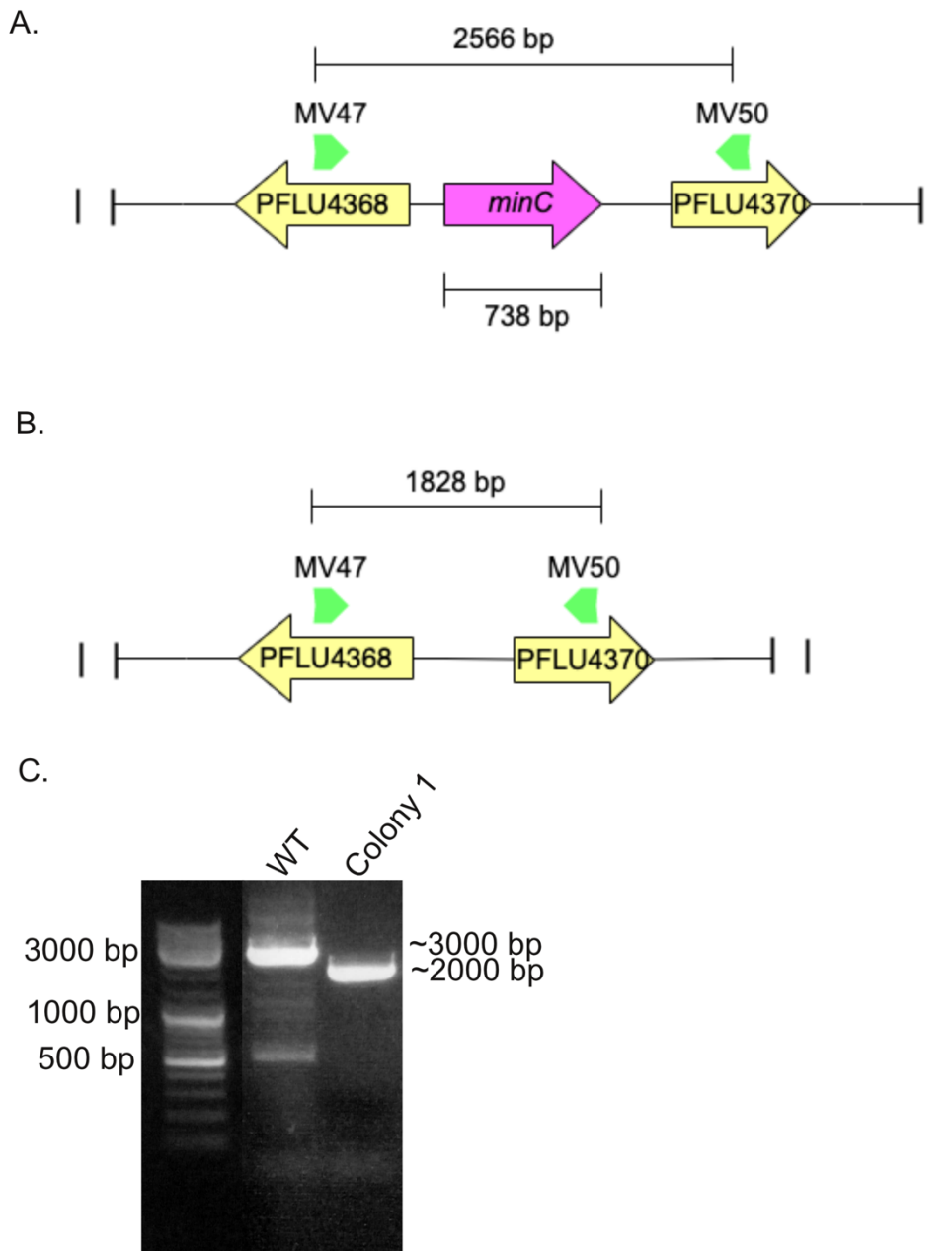


Fig. 7: *minC* was deleted from the SBW25 genome. A) Representative image showing the size and location of the region to be deleted, along with the primers used to confirm the deletion. B) Expected product size, if the deletion is successful. C) Colony-PCR gel image showing the confirmation of deletion.

Genome sequencing of $\Delta minC$ SBW25 showed the absence of compensatory mutations:

Previous attempts at disrupting *minC* in *Pseudomonas fluorescens* failed (Price et al., 2018), as they did in *P. aeruginosa* (Poulsen et al., 2019) in rich medium (the conditions used in this study). We were therefore concerned that the $\Delta minC$ strain may have survived due to a compensatory mutation elsewhere in the genome. To check if any other mutations were present, we sequenced the entire genome of the $\Delta minC$ mutant using Illumina short read sequencing (Fig. 8A). The reads obtained were paired and aligned to the reference genome of *P. fluorescens* SBW25.

1,923,733 out of the 1,929,782 reads obtained were aligned to the reference with an average coverage per site of 42.0 ± 9.4 (Fig. 8B). No candidate compensatory mutations were observed. Other than the deletion of *minC* and two background mutations (differences between the reference genome and the lab strain of SBW25), no mutations were detected (Fig. 8C).

Characterisation of *minC* mutants:

The consequences of *minC* deletion on the phenotype and fitness of the cell, were understood by measuring its cell morphology parameters and comparing it to that of the WT. The relative fitness of the mutant with respect to the WT was also measured.

a) $\Delta minC$ mutants grown in LB medium have diverse cell morphologies

The phenotypical consequences of *minC* deletion and how it compares with the WT strain was identified by visualising WT and $\Delta minC$ cells under the microscope. Membrane dye (FMTM4-64) staining was used to improve the accuracy of the measurements. Cells exhibited a variety of cell morphologies. Many cells showed the asymmetric formation of division septa, which resulted in the formation of long cells and minicells. Cells which had Y-shaped ends were also rarely seen (Fig 9).

b) $\Delta minC$ mutants had a less severe phenotype in M9 minimal medium than in LB medium.

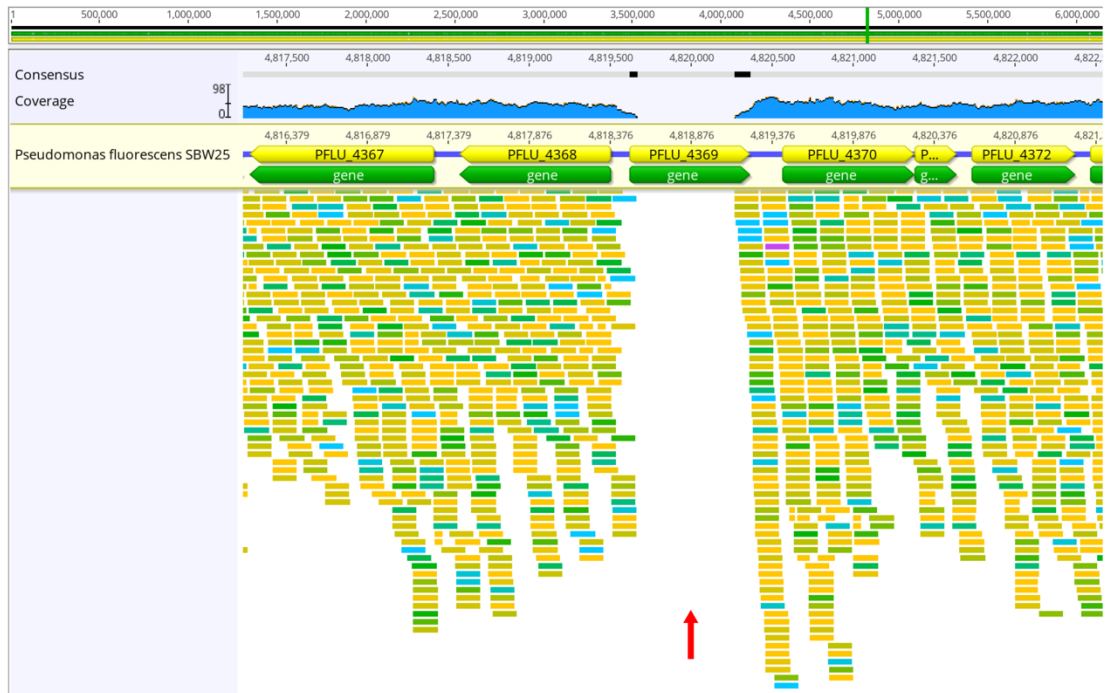
Recently, MinC was shown to be essential in rich medium, but not in minimal media for *P. aeruginosa* suggesting that the magnitude of the effects of the mutation depend on the environment. Hence, we checked if the cell division

defect of $\Delta minC$ mutants was less pronounced in minimal medium (Fig. 10B) than in rich medium (Fig. 10A). Cell morphology parameters: length (Fig. 11A) and width (Fig. 11B) of the wildtype and $\Delta minC$ in both media were measured by analysing cell outline data produced by the JFilament plugin of ImageJ (see Methods). In each medium, $\Delta minC$ mutants found to be longer and wider than the respective wildtype cells. Both genotype and environment were significant predictors of cell size. $\Delta minC$ cells were longer in both LB ($6.97 \pm 0.21 \mu\text{m}$) and M9 ($2.21 \pm 0.07 \mu\text{m}$) than were WT cells (LB: $2.67 \pm 0.03 \mu\text{m}$; M9: $1.64 \pm 0.02 \mu\text{m}$). Mutants were also wider in both LB ($0.808 \pm 0.004 \mu\text{m}$) and M9 ($0.650 \pm 0.004 \mu\text{m}$) than were WT cells (LB: $0.548 \pm 0.002 \mu\text{m}$; M9: $0.458 \pm 0.002 \mu\text{m}$). Thus, averaged across environments, $\Delta minC$ cells were 1.9 -x longer and 1.1-x wider than WT cells. Additionally, cells of both genotypes were an average of 3.1-x longer and 1.5-x wider when grown in LB than in M9. Differences in cell length and width between the WT and the mutant were greater than would be expected by chance alone ($P < 0.0001$). Post hoc Tukey HSD tests revealed significant differences between the two strains.

c) Loss of MinC function had a large fitness cost in LB medium

To check for fitness effects of the point and deletion mutants, we tagged the wildtype, and $\Delta minC$ mutants with GFP and RFP separately and measured the number of cells of each kind at two different time points using fluorescent flow cytometry. The fitness effect of having two different fluorophores was checked by competing each GFP tagged strain of WT and $\Delta minC$ against their RFP counterparts. Differently tagged counterparts of each strain had a relative fitness close to 1, indicating there was no fitness effect of the marker. Competing $\Delta minC$ RFP against the wildtype GFP and vice versa revealed the relative fitness between $\Delta minC$ RFP and wildtype GFP to be 0.931 ± 0.014 and $\Delta minC$ GFP and wildtype RFP to be 0.930 ± 0.015 respectively (Fig. 12). These differences were higher than would be expected by chance ($P < 0.0001$). Post hoc Tukey HSD tests revealed significant differences between the mutant and the wildtype.

A.



B.

Total no of reads	Total no of reads mapped	Average coverage
1,929,782	1,923,733	42.0 ± 9.4 (Max:98, Min:0)

C.

Position in the genome	Mutation	Description
45,881	Δ1bp	Background mutation in the strain
3,447,984	+G	Background mutation in the strain
4,818,500	Δ738bp	Deletion of <i>minC</i> (PFLU4369)

Fig. 8: Illumina sequencing confirmed the deletion of *minC* and absence of compensatory mutations. A) Illumina sequenced reads aligned to the reference *P. fluorescens* SBW25 genome using Geneious Prime™. Red arrow indicates the absence of reads and coverage for *minC* gene (PFLU4369). B) Statistics of the alignment C) Mutations obtained after checking for variants/SNPs.

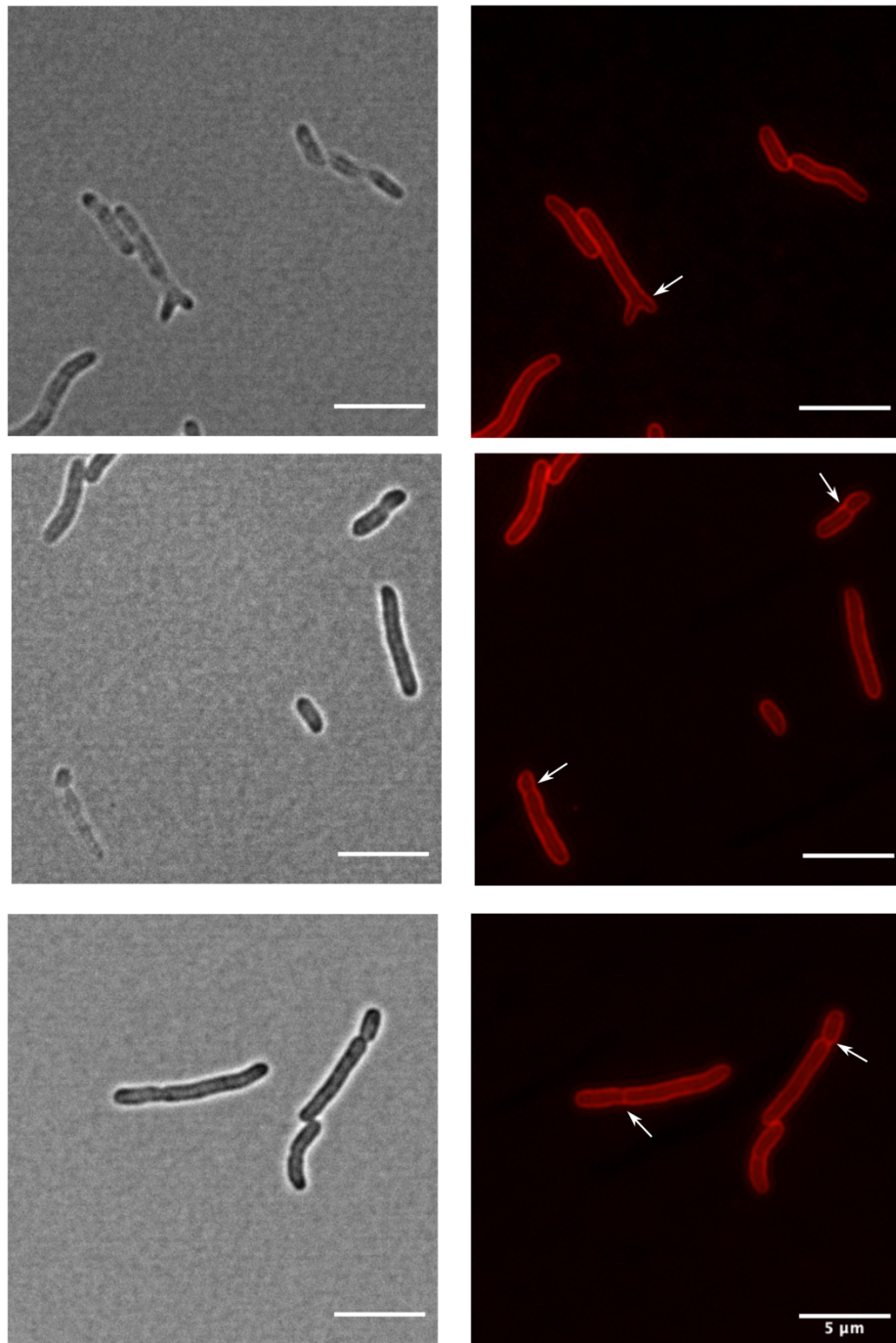


Fig. 9 : $\Delta minC$ cells had a diversity of cell morphologies. Brightfield and membrane stained (FM[™]4-64) stained images of $\Delta minC$ cells grown in LB medium. Scale bar = 5 μ m Observed morphologies included cells with Y-shaped ends, an asymmetric formation of division septa. Disproportionately long cells and minicells were also present.

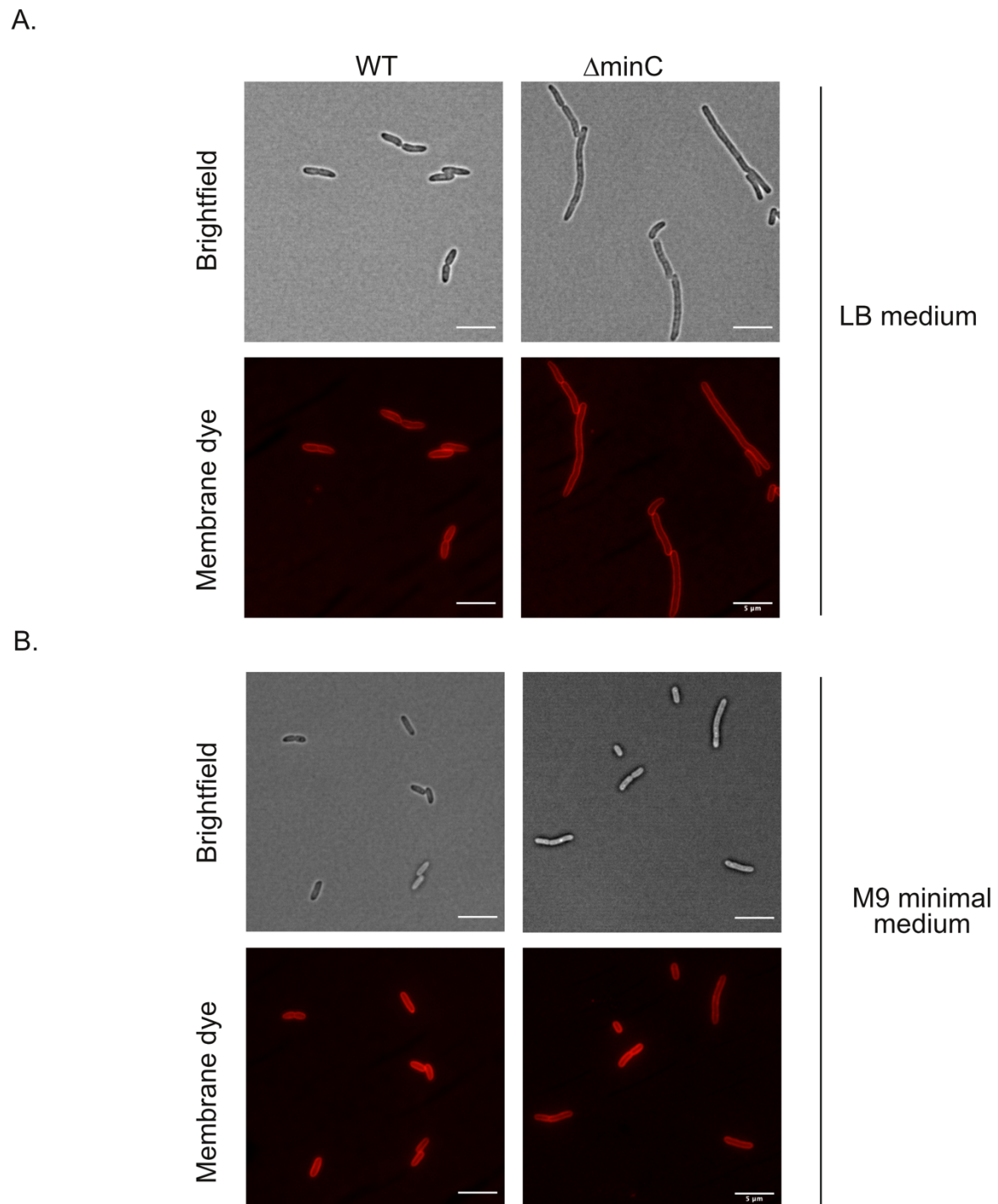
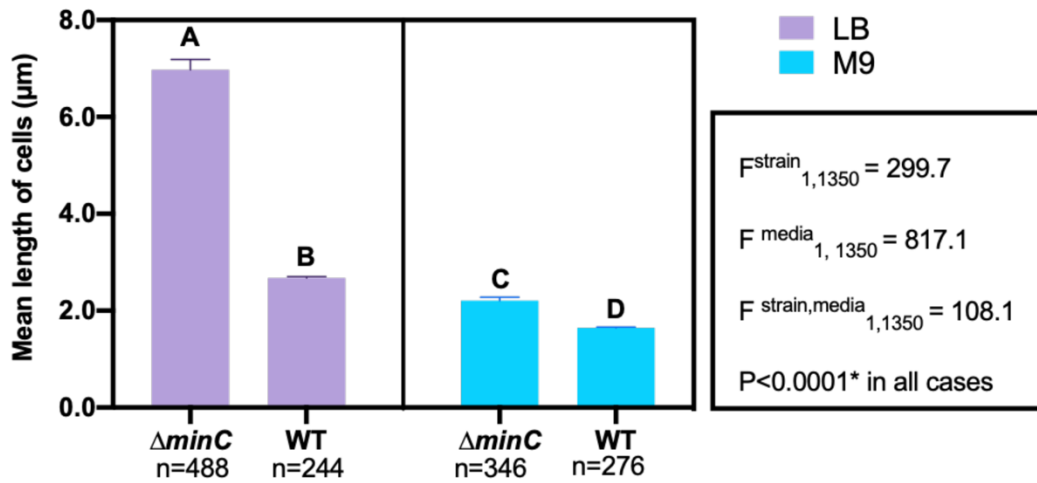


Fig. 10: A difference in severity of phenotype of the *minC* deletion was seen when mutants were grown in LB and M9 minimal media. Brightfield and membrane stained(FMTM4-64) images of wildtype and $\Delta minC$ strains grown in A) LB medium and B) M9 minimal medium. Scale bar = 5 μ m.

A.



B.

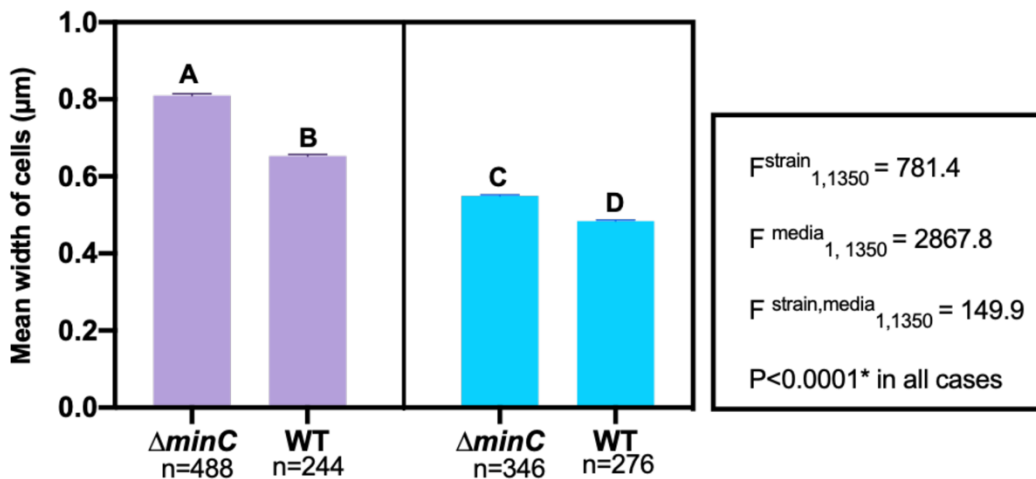


Fig. 11: $\Delta minC$ cells are longer and wider than wildtype cells in LB and M9 minimal medium. However, $\Delta minC$ has a more severe phenotype in LB than in M9 minimal media. Mean A) length and B) width of $\Delta minC$ and WT cells in LB and M9 minimal media respectively. Three biological replicates were used for the measurements. Total number of cells counted (n), as mentioned. Error bars indicate SEM. F-statistic for the parameter(s) explaining the variance as depicted. Measures indicated by a different letter are significantly different according to the Tukey HSD test. $P < 0.05$.

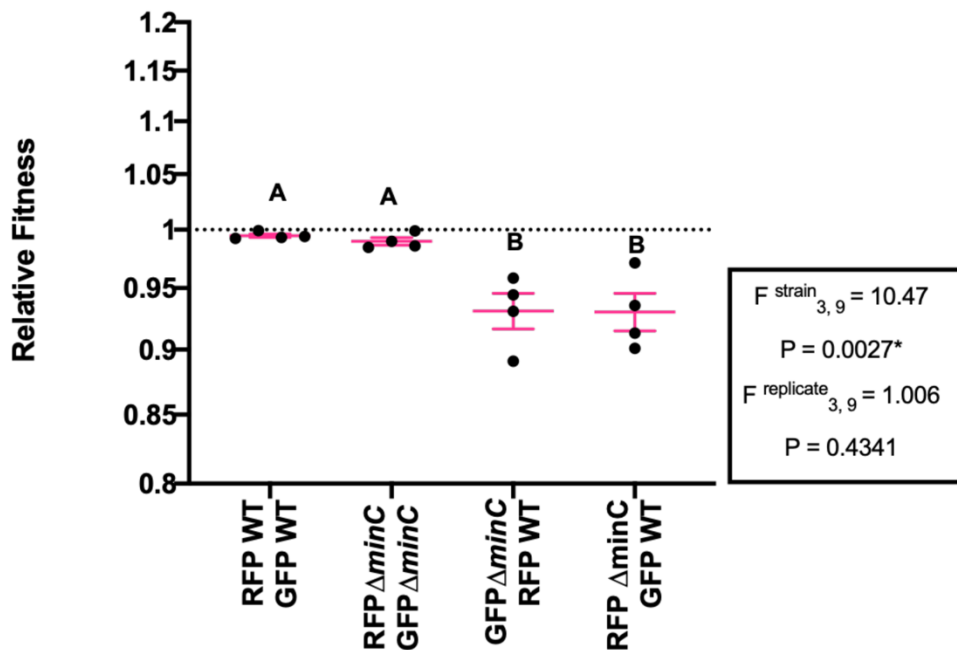


Fig. 12: $\Delta minC$ strain was less fit than the wildtype strain . A) Relative fitness measures of the RFP tagged strain against the GFP tagged strains of wildtype and $\Delta minC$ amongst and against each other. Four biological replicates were used. Error bars represent SEM. F-statistic for parameter(s) explaining/not explaining the variance as depicted. relative fitness. Measures indicated by a different letter are significantly different as per the Tukey HSD test. $P < 0.05$.

GFP tagged *minC* was constructed in *P. fluorescens* SBW25

MinC oscillations have been observed in *E. coli* by tagging the protein with a fluorescent marker on the N-terminus. To understand the dynamics of MinC in *P. fluorescens* SBW25, we attempted to replicate this by tagging the MinC orthologue wildtype with msfGFP. *msfGFP* was attached to the 5' end of *minC* gene using an N-terminal linker sequence that coded for the residues SGGGG. We screened colonies obtained after cycloserine enrichment using colony PCR with two primers that flanked the region where the insertion is to take place, to confirm the insertion (Fig. 13A). A 1.0 kb product is obtained if the insertion is unsuccessful (Fig. 13A) and a 1.8 kb product is obtained for a successful insertion (Fig. 13B). Agarose gel electrophoresis showed that the amplified fragment was around 1.8 kb (Fig. 13C). Insertion was confirmed by Sanger sequencing.

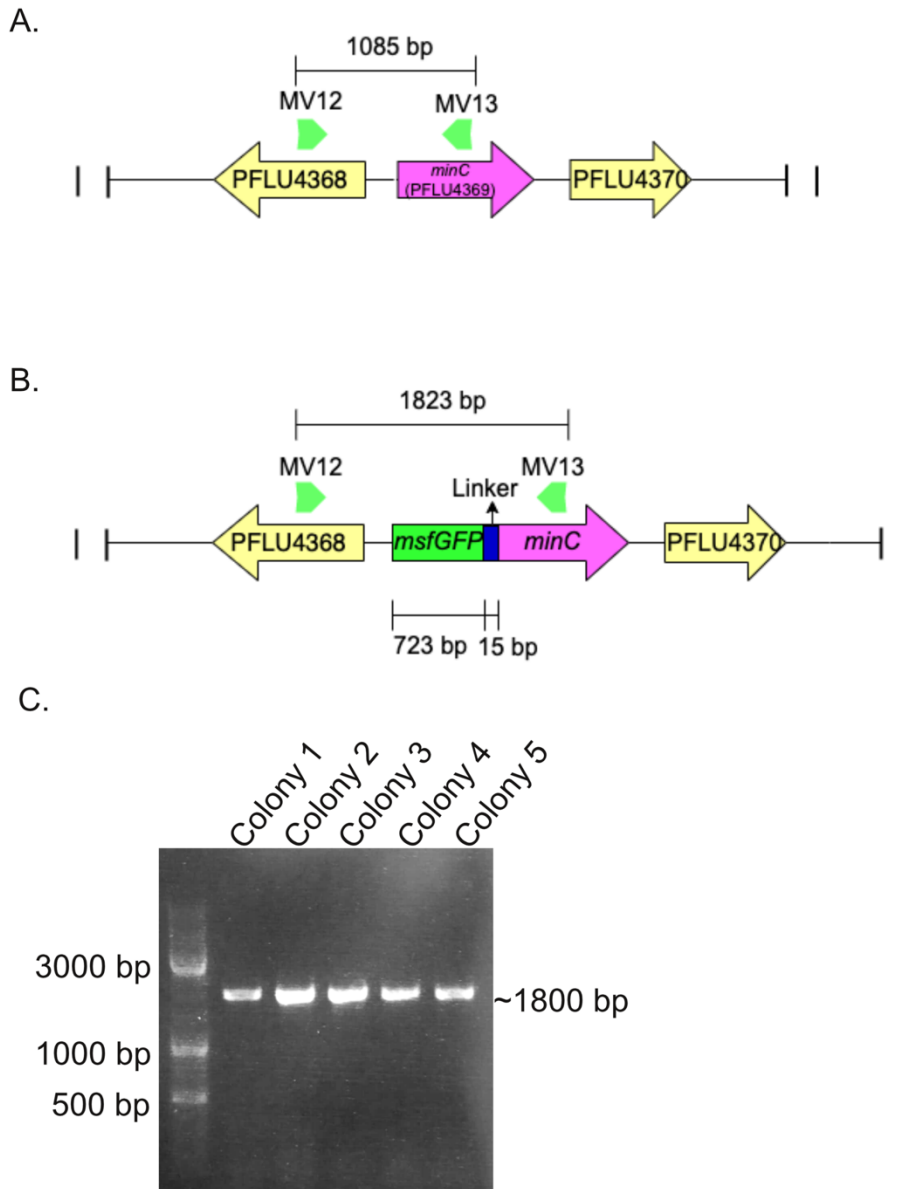


Fig. 13: *msfGFP-minC* was constructed in the SBW25 genome. A) Representative image showing the site of insertion of *msfGFP* and the linker sequence, along with the primers used to confirm the insertion and expected product size if insertion is unsuccessful. B) Expected product size if the insertion is successful. C) Colony-PCR gel image showing the confirmation of insertion.

Endogenous *msfGFP* tagged MinC gave a weak signal

WT and *msfGFP*-MinC cells were visualised under the microscope to assess the behaviour of the *msfGFP*-MinC in the tagged strain. Brightfield, GFP and DAPI channels were used to visualise the cells. DAPI channel was used to check the presence of pyoverdine, a fluorescent molecule that is produced by *P. fluorescens*

SBW25 and tend to localise on the poles of the cell in the absence of iron. Pyoverdine is also suspected to interfere with the fluorescence signal of GFP. WT grown in the absence of iron served as a positive control for the presence of pyoverdine, hence a positive signal from the DAPI channel (Fig. 14A), while WT grown in the presence of iron served as a negative control for the presence of pyoverdine, hence a negative signal from the DAPI channel and a negative control for GFP signal as well. (Fig. 14B). msfGFP-MinC cells were grown in the presence of iron to avoid false signal from pyoverdine (Fig. 14C). The msfGFP-MinC cells failed to give a strong GFP signal and looked similar to the negative control.

Inducible msfGFP-MinC plasmid was constructed

The failure of msfGFP-MinC to give a positive signal, when it was expressed endogenously, led to the need to confirm that the construct msfGFP-MinC fusion made was functional. For this, we inserted the N-terminal linker attached MinC in to the C-terminal of msfGFP under a cyclohexanone inducible promoter. The inducible system produces a protein (ChnR) that binds to the promoter (*PchnB*) and activates translation of the downstream gene. To confirm the insertion, we screened colonies obtained after electroporation using colony PCR with two primers that flanked the region where the insertion is to take place (Fig. 15A). An unsuccessful insertion will give a 490 bp product (Fig. 15A) while a successful insertion will give a 1.2 kb product (Fig. 15B). Amplified fragment was around 1.2 kb, as per gel electrophoresis results (Fig. 15C). Insertion was confirmed by sanger sequencing.

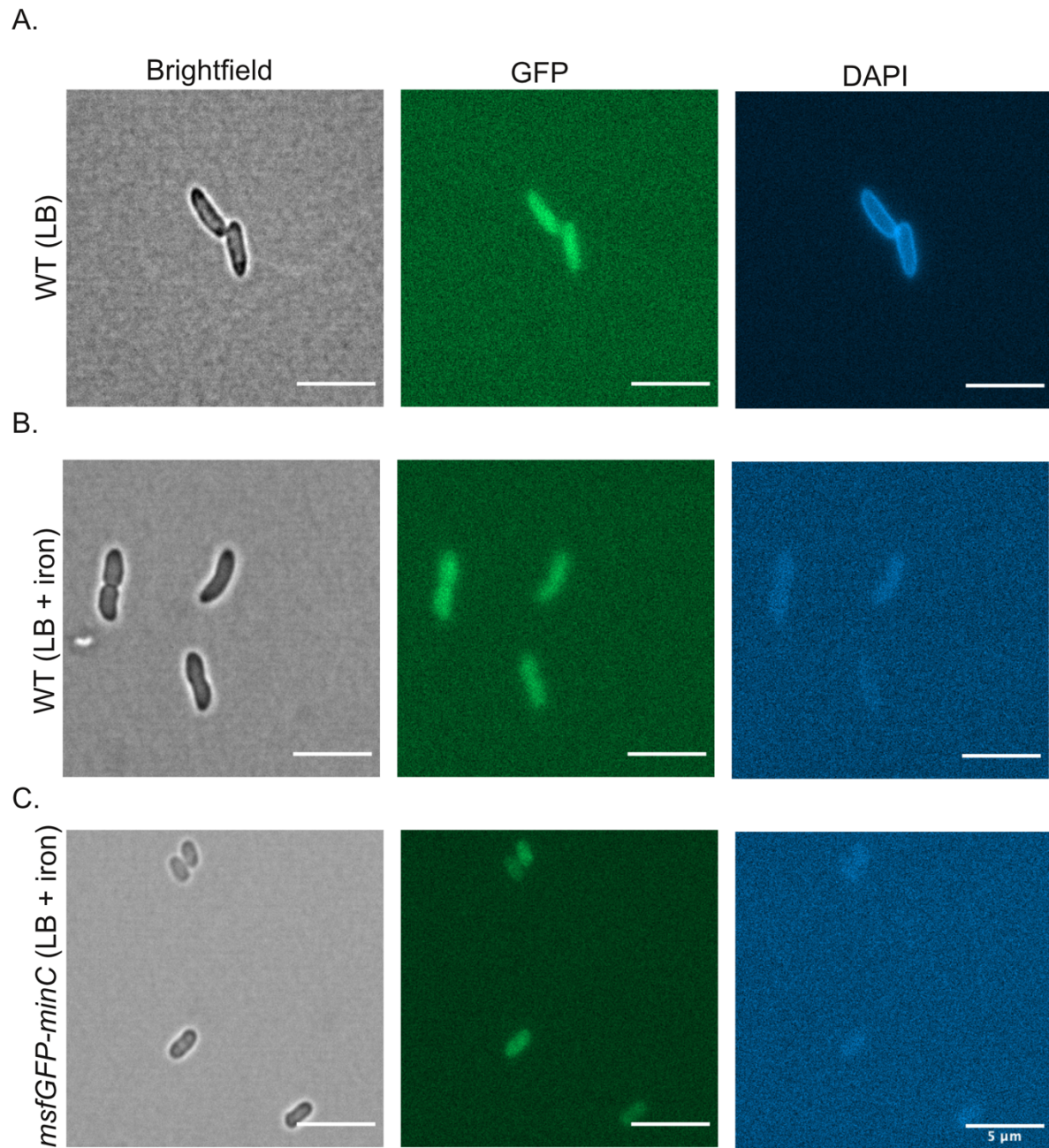


Fig. 14: *msfGFP-MinC* did not give a prominent GFP signal. Brightfield, GFP and DAPI images of A) WT grown on LB, B) WT and C) *msfGFP-MinC* strains grown on LB media supplemented with iron. Scale bar = 5 μ m. Exposure time for GFP channel = 200 ms and DAPI channel = 150 ms.

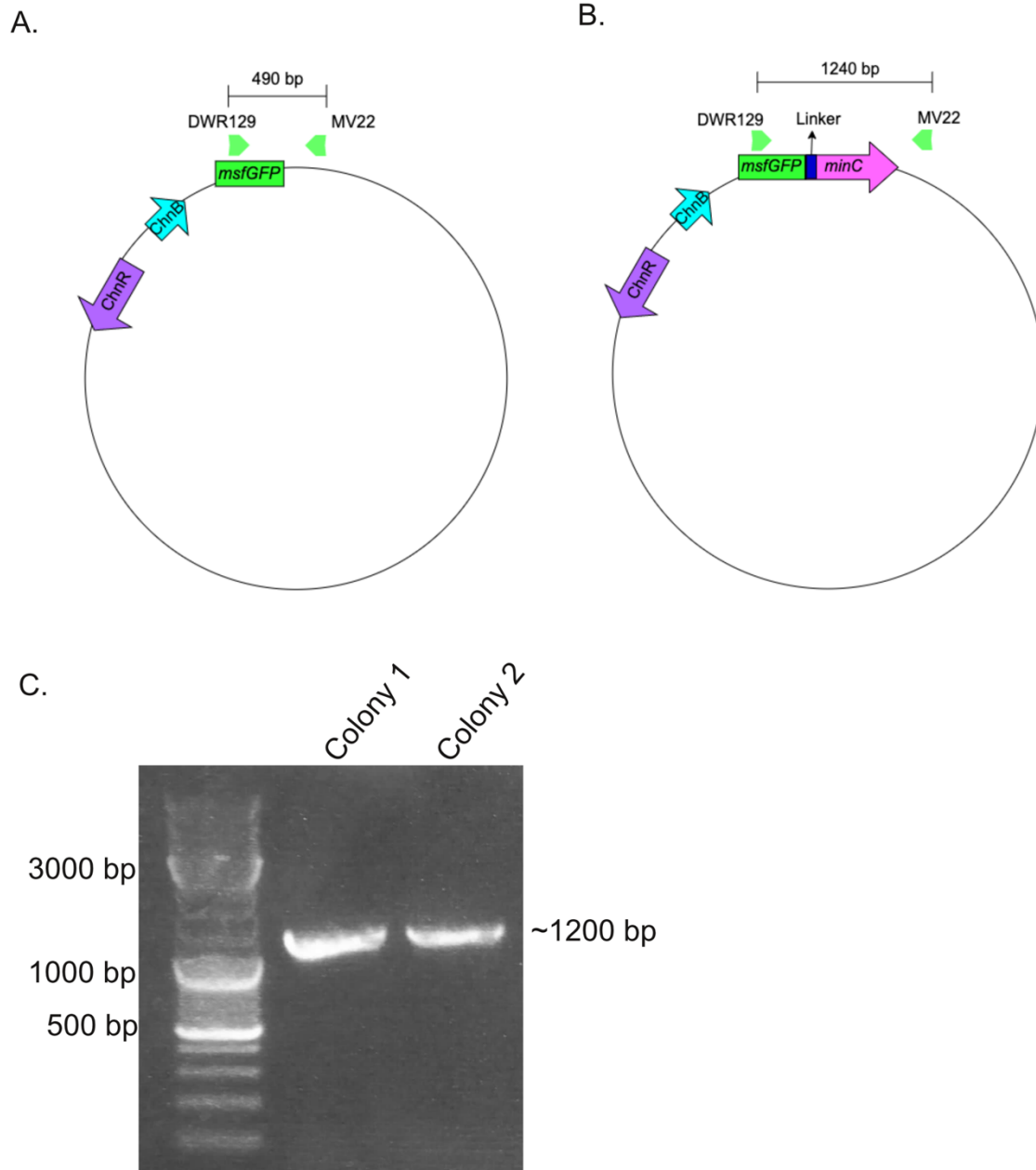


Fig. 15: *msfGFP-minC* gene was inserted under a cyclohexanone inducible promoter in the pSCM plasmid. A) Representative image showing the site of insertion, along with the primers used to confirm the insertion and expected product size if the insertion is unsuccessful. B) Expected product size, if the insertion is successful. C) Colony-PCR gel image showing the confirmation of insertion.

Expression of msfGFP-MinC via plasmid generates elongate green cells

The functionality of the msfGFP-MinC in the inducible msfGFP-MinC transformed strain (p-chn msfGFP-MinC) was checked. For this, we visualised WT and p-chn msfGFP-MinC cells under the microscope. Brightfield, GFP and DAPI channels were used to visualise the cells. DAPI channel was used for the same reason as mentioned above. WT grown in the absence of iron served as a positive control for the presence of pyoverdine, hence a positive signal from the DAPI channel (Fig. 16A), while WT grown in the presence of iron served as a negative control for the presence of pyoverdine, hence a negative signal from the DAPI channel and a negative control for GFP signal as well. (Fig. 16B). p-chn msfGFP-MinC cells were grown in the presence of iron to avoid false signal from pyoverdine (Fig. 16C). The msfGFP-MinC cells were 10 to 20 times longer than the wildtype cells and gave a strong GFP signal even in the absence of the inducer cyclohexanone. Thus, we could confirm the expression and functionality of both msfGFP and MinC since the cells were bright green and extremely long, respectively. Unfortunately, expression was so strong, even in the absence of the inducer, that we could not use these strains to characterize the function on MinC in SBW25.

Tn-7 inducible fluorescent tagged *minC* in wildtype and $\Delta minC$ strains were constructed

For limiting the amount of msfGFP-minC produced via the inducible plasmid in the cell, we decided to insert the cyclohexanone inducible system in to the genome of the WT and $\Delta minC$ strains, thereby reducing the number of copies of the construct per cell compared to the strains bearing the plasmid. For this we used the Tn7 transposon system, capable of inserting itself in the *glmS* gene of *P. fluorescens* SBW25. To confirm the insertion, we screened colonies obtained after electroporation using colony PCR with two sets of primers, one that flanked the region including a part of the inducible system and the *glmS* gene (Fig. 17B) and the other, a region within the inducible system (Fig. 17C). An unsuccessful insertion will give no product (Fig. 17A) while a successful insertion will give a 700 bp product for the first set of primers (Fig. 14B) and 1500 bp product for the second set of primers (Fig. 17C). Amplified fragments were around 700 bp (Fig. 17D) and 1500 bp (Fig. 17E) respectively as shown by gel electrophoresis. Sanger sequencing of the obtained products confirmed the insertion in both the strains.

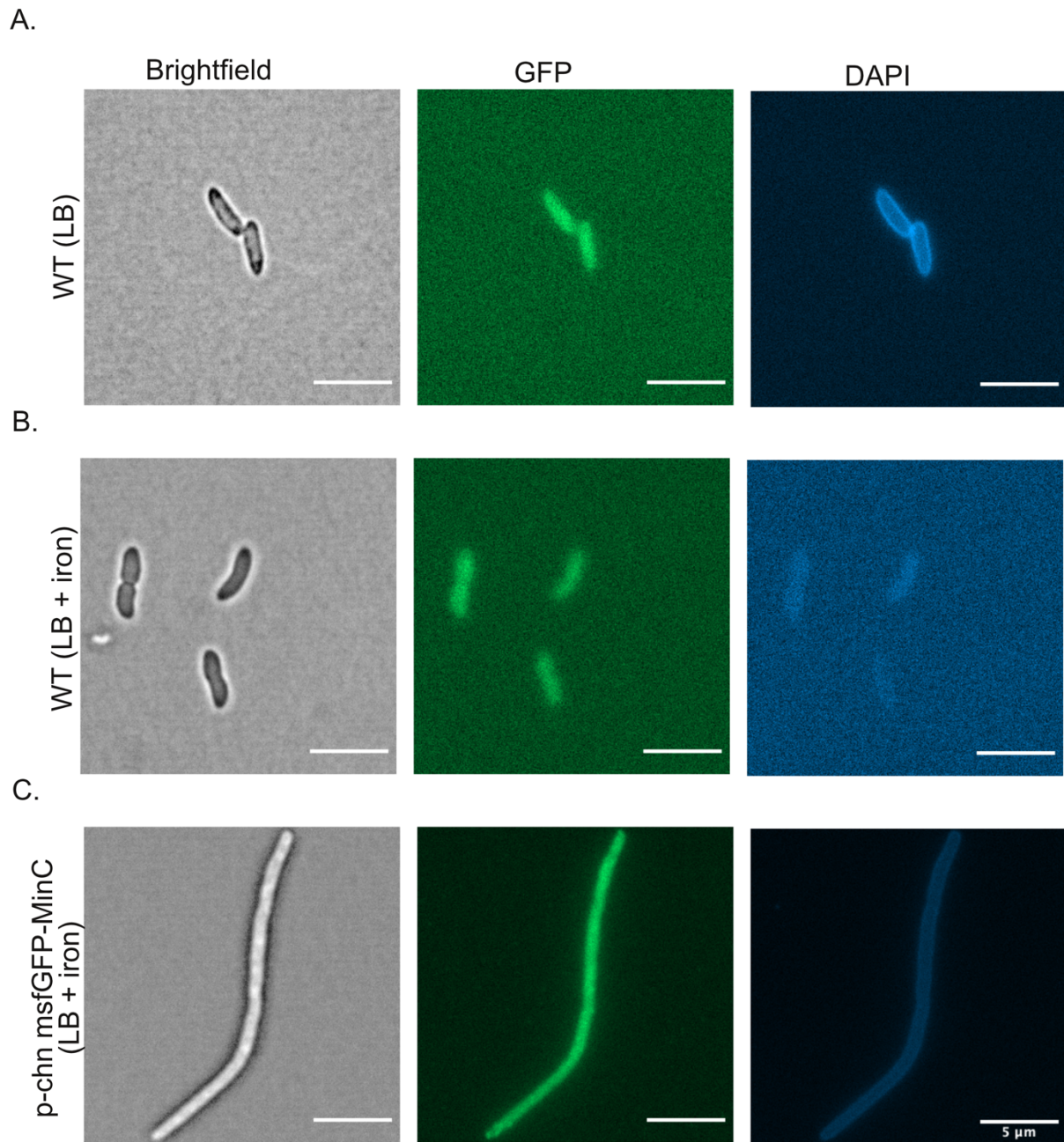


Fig. 16: Cyclohexanone inducible msfGFP-MinC transformed strain overexpressed msfGFP-MinC, even in the absence of the inducer. Brightfield, GFP and DAPI images of A) WT grown on LB, B) WT and C) Cyclohexanone inducible msfGFP-MinC plasmid (p-chn msfGFP-MinC) transformed strains grown on LB media supplemented with iron. Scale bar = 5 μm. Exposure time for GFP channel = 200 ms and DAPI channel = 150 ms.

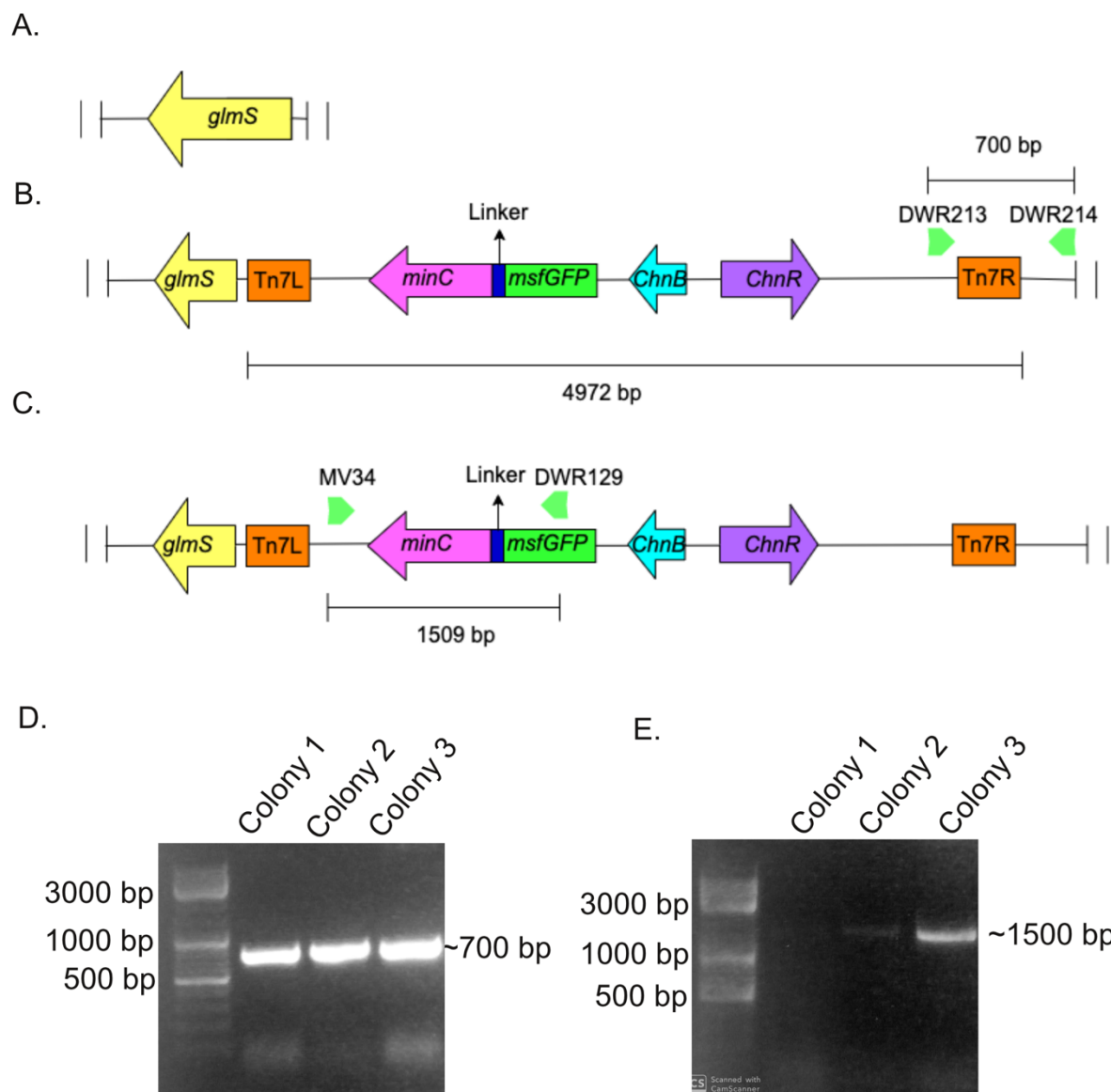


Fig. 17: Cyclohexanone inducible *msfGFP-minC* gene was inserted in *glmS* gene via Tn7 mediation. A) *glmS* gene. Representative image showing the location and size of the insertion, along with B) first set of primers and C) second set of primers used to confirm the insertion and expected product sizes if the insertion is successful. No product is obtained using the above set of primers, if insertion is unsuccessful. Colony-PCR gel image showing the confirmation of insertion by D) first and E) second set of primers.

Tn-7 inducible msfGFP-MinC localised to the poles/ prospective poles in WT and $\Delta minC$ cells respectively

The functionality of the msfGFP-MinC in the inducible msfGFP-MinC was checked by visualising WT and WT-Tn7 msfGFP-MinC and $\Delta minC$ -Tn7 msfGFP-MinC cells under the microscope using Brightfield, GFP and DAPI channels. DAPI channel was used for the same reason as mentioned above. WT (Fig. 18A), WT-Tn7 msfGFP-MinC (Fig. 18B) and $\Delta minC$ -Tn7 msfGFP-MinC (Fig. 18C) were grown in the presence of iron without and with the inducer (0.01 μ L of 2% cyclohexanone). The optimal amount of inducer was found by the inducer assay (see methods). The WT served as the negative control. WT-Tn7 msfGFP-MinC strain grown in the presence of inducer were longer and showed the localisation of msfGFP-MinC in one pole of the cell (Fig.18B (+ inducer)), while the cells grown in the absence of the inducer were shorter and gave a GFP signal similar to the negative control (Fig.18B (- inducer)). $\Delta minC$ -Tn7 msfGFP-MinC cells were 10-20 times longer, undivided and showed regularly interspaced localisation of msfGFP-MinC in the potential poles (Fig.18C (+ inducer)), while the cells grown in the absence of the inducer were shorter(although characteristically longer than the WT) and gave a GFP signal similar to the negative control (Fig.18C (- inducer)).

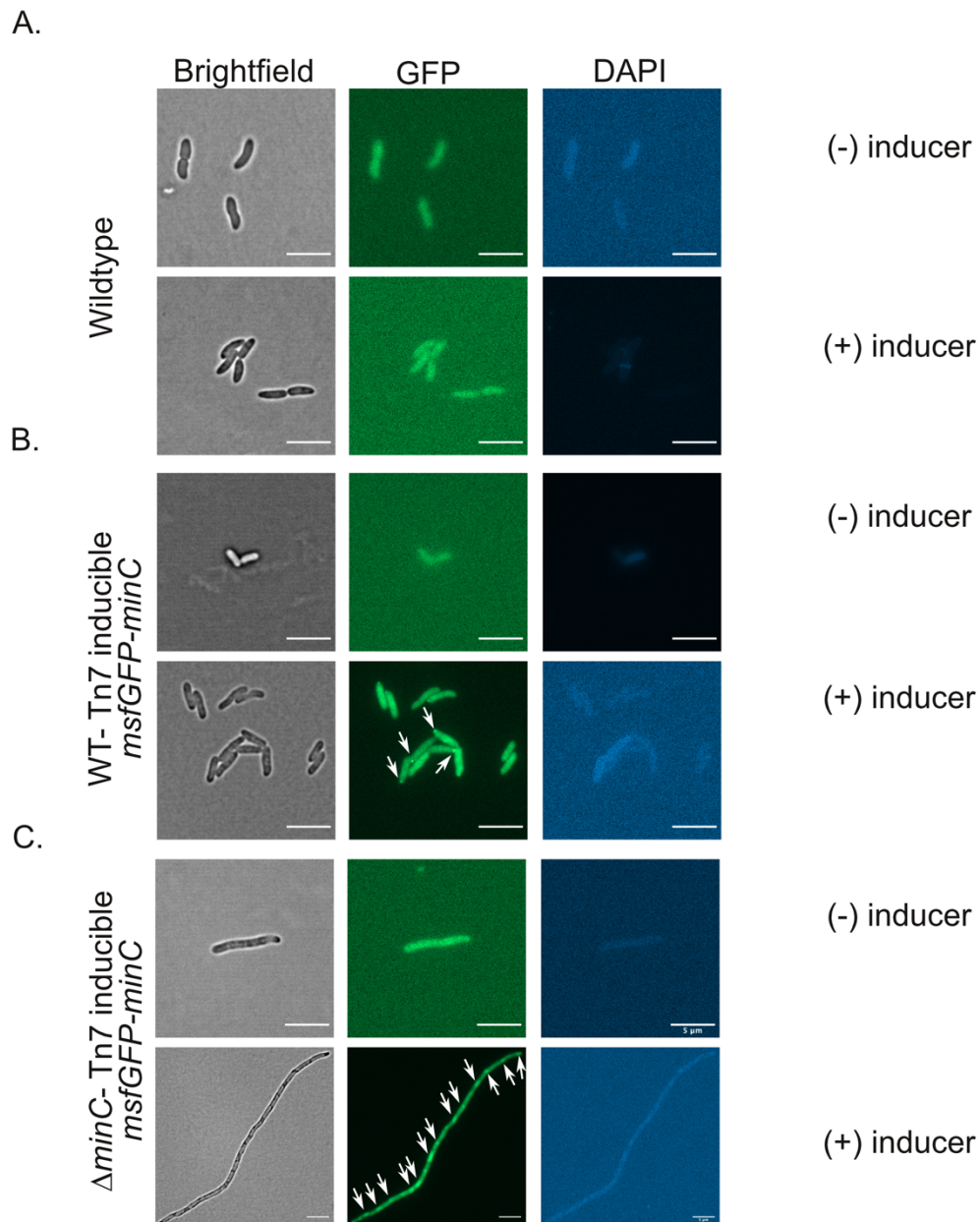


Fig. 18: *msfGFP*-MinC localised to the pole and potential poles in WT-Tn7 inducible *msfGFP*-MinC and Δ *minC*-Tn7 inducible *msfGFP*-MinC respectively. Brightfield, GFP and DAPI images of A) Wildtype with no inducer and added inducer. B) WT-Tn7 inducible *msfGFP*-MinC with no inducer and added inducer. C) Δ *minC*-Tn7 inducible *msfGFP*-MinC with no inducer and added inducer. Scale bar = 5 μ m. Strains grown on LB media supplemented with iron. 0.01 μ l of 2% cyclohexanone was the inducer. Exposure time for GFP channel = 200 ms and DAPI channel =150 ms.

DISCUSSION

This study attempted to understand the function of proteins involved in bacterial cell shape and division in the context of evolution. The study particularly focussed on answering the questions that arose from the evolved spherical $\Delta mreB$ mutant of *P. fluorescens*. First of these findings is the difference established between the point and deletion mutant of *pbp1A*, which have implications in understanding how the $\Delta mreB$ mutants regain their fitness after 1000 generations of evolution. Second and most important finding is the identification of the cell division inhibitor MinC in *P. fluorescens* SBW25, establishing MinC is essential for ensuring proper cell division in SBW25 and investigating its localisation in the cell can help us understand how the $\Delta mreB$ mutants divide. The study has also provided more insights on improving selection techniques in molecular cloning, microscopy and cell measurement procedures.

Comparing *pbp1A* deletion mutant and the *pbp1A* (G1450A) mutant revealed differences in width and area of the cell. Both mutants were different from the wildtype in terms of length, width and area. However relative fitness for all strains were found to be the same. This observation shows that the compensatory point mutation that evolved in *pbp1A* gene in the $\Delta mreB$ mutant, leading to corresponding to an amino acid substitution (D484N) in the transpeptidation site of the protein is not equivalent to a loss of function mutation. This is contrary to the speculations of (Yulo et al., 2018) that it is a loss of function mutation which was based on the observation that a similar mutation T371A in the transpeptidation site of PBP1a in *S. pneumoniae* decreased its reactivity to β -lactams, which resemble the natural substrate of PBP1a: peptidoglycan (Job et al., 2008). A point mutation in the transpeptidation site of *pbp1A* may not result in a complete loss of function of the protein as the glycosyl transferase domain of the protein could still be functional. Moreover, some proteins that have point mutations in their active site have been shown to acquire an altered function (Bhuvanachandra et al., 2018; Rignall et al., 2002). It also seems likely that if loss of PBP1a function could compensate for the deletion of *mreB*, that Yulo et al. (2018) would have observed a large number of nonsense or frameshift mutations alongside the point mutations characterized. Instead, the point mutation in *pbp1A* may cause a structural and a consequent functional change in the protein, the effects of which is amplified by the inactivation of MreB.

The rod complex is believed to be the main machinery involved in transpeptidation and transglycosylation in the polymerisation of peptidoglycan, while PBP1a diffuses around the cell and fixes any gaps formed in the peptidoglycan layer caused by mechanical stress (van Teeffelen and Renner, 2018). Inactivation of MreB might result in a decreased efficiency in the functioning of the rod complex, which results in an ill formed peptidoglycan layer, in addition to effects from mechanical stress. Hence, the point mutation in transpeptidation site of *pbp1A*, might be improving the efficiency of its ability to perform transpeptidation owing to the inefficiency of the main machinery to do so. This could explain why the fitness effect of the point mutation is negligible in the wildtype background, where an efficient mechanism to do so already exists. Deleting *pbp1A* in the Δ *mreB* mutant will provide more insight about the actual effect of the point mutation and allow direct investigation of the above hypothesis. Finally, an important caveat is that the cell measures reported in this study were obtained by from a single overnight culture of each strain and need to be replicated to ensure they are repeatable. That being said, the decrease in width noticed for *pbp1A* (G1450A) mutants here is comparable to that noticed by (Yulo et al., 2018), suggesting that the single replicate is representative.

Δ *mreB* cells divide asymmetrically, but rapidly evolved to divide symmetrically under serial passage (Yulo et al., 2018). The ability of rod-shaped cells to divide symmetrically is attributed to the MinCDE system, which is an ATPase based cell division control machinery (Lutkenhaus, 2007). Not much is known about the function of MinC in SBW25; even the viability of Δ *minC* mutants in *Pseudomonas* was subject to conflicting reports. While one study (Carter et al., 2017), established that Δ *minC* mutants in *P. aeruginosa* were viable in rich media, another study (Poulsen et al., 2019) speculated that MinC is essential in nutrient rich medium, but not in minimal media. Tn5 mediated mutations in MinC have also not been reported in *P. fluorescens* (Price et al., 2018). Our first few attempts to obtain Δ *minC* mutants via two step allelic exchange resulted in failure, which almost persuaded us to conclude that MinC was essential for the cell and the resulting mutants would not be viable. However, we did eventually generate a Δ *minC* mutant in SBW25, surprisingly in rich medium. The difficulty to obtain the mutant and studies claiming it was essential raised the possibility that the mutant carried compensatory mutations, allowing its survival. To check for this, we sequenced the genome of the Δ *minC* mutant and found no other mutations.

The $\Delta minC$ mutant had a huge fitness defect of about 7% relative to the wildtype in nutrient rich medium. This likely explains why Price et al (2018) failed to observe *minC* mutants via Tn5 mediated mutagenesis. Their approach identified mutants by amplicon sequencing barcodes attached to the transposon and therefore has little power to detect rare unfit mutants. The phenotype of $\Delta minC$ mutants in rich media included elongate cells, asymmetric formation of division septa and minicells consistent with phenotype observed in *E. coli* (de Boer et al., 1989) and *P. aeruginosa* $\Delta minC$ mutants (Carter et al., 2017). Unusual Y-shaped cells were also seen, as reported in the $\Delta minC$ mutant of *A. tumefaciens* (Flores et al., 2018). The phenotype of the mutant was found to be especially severe in rich media compared to minimal media. These differences were more exaggerated in the mutants than wildtype indicating that the severity of phenotype is a synergistic effect of the genotype and the environment.

Difference in severity of phenotype based on environment have been noticed before in *B. subtilis* (Levin et al., 1998), where they observed that majority of the $\Delta minCD$ cells had a properly positioned Z-ring in minimal medium, as opposed to the presence of multiple Z-rings in rich medium. The authors attribute this to the presence of additional division controlling factors in the cell, whose functions are more prominent in minimal medium. Bacterial cells take longer to divide in M9 minimal medium compared to LB medium (Figure. 1 in (Li et al., 2014)). Slower division would mean that the additional machinery that controls the formation of the Z-ring might be able to catch up and help divide the cell before they are long, although not as accurately as MinC. Additional mechanisms might not correct division in LB medium where cells are able to grow faster and would already be long before the additional machinery kicks in. The efficiency of the additional control mechanism would therefore be limited by the growth rate of the cell. Assessing the relative fitness of the $\Delta minC$ mutants compared to wildtype grown in M9 minimal medium may provide more insight on the existence of an additional mechanism for Z-ring formation control and its greater efficiency in minimal medium. The viability of $\Delta minC$ cells shows that such mechanisms must exist. One candidate is nucleoid occlusion, which has been shown to play a role in the correct placement of cell division in *E. coli* and *B. subtilis*. Additional mechanisms apart from these, also exist in these two organisms (Pinho et al., 2013).

One way we can check for this is to visualise the nucleoid in these $\Delta minC$ cells, which might shed more light on the sequestration of genomic DNA and prevalence of nucleoid occlusion in SBW25.

Experimental evolution can help to identify the nature of additional mechanisms allowing symmetrical division. Long-term evolution in $\Delta mreB$ mutant proved useful in identifying other players involved in the maintenance of cell shape. Therefore, we can get insight on other mechanisms of cell division by performing a long-term evolution experiment on $\Delta minC$ mutants which might reveal compensatory mutations that restore symmetric division in the mutant. Furthermore, we observed that the $\Delta minC$ mutants in SBW25 have a distinct colony morphology compared to the wildtype. Performing a Tn5 mediated suppressor mutagenesis (Fellay et al., 1989) on them and screening wildtype revertant colonies could also identify compensatory mutations.

The behaviour and localisation of MinC in SBW25 was investigated by fluorescent tagging the protein with msfGFP. As described by previous studies, MinC is expected to localise on one of the poles of the cell like in *E. coli*, or both poles like in *B. subtilis* (Lutkenhaus, 2007). When endogenously expressed msfGFP-MinC was visualised, bright green signals were seen on the poles of the cell. However, this was found to be pyoverdine, an iron scavenging fluorescent molecule produced by *P. fluorescens* (Moon et al., 2008). To reduce the fluorescent signal stemming from pyoverdine, msfGFP-MinC SBW25 was grown in the presence of iron. This time we failed to see any bright green signals from the poles, indicating that the construct was not producing a visible product either because expression was too weak or the product was not functional.

The functionality of the construct was confirmed when we could express it via a plasmid under a cyclohexanone inducible promoter. This time we saw elongate bright green cells, even in the absence of the inducer. msfGFP-MinC was overexpressed in the cell, possibly the result of having a large copy number of plasmids in the cell which could not give us any information on the localisation of MinC. Hence, we captured two ends of the spectrum: the endogenous promoter generated too weak a signal to visualize while the plasmid-borne inducible promoter was so leaky that it generated an extremely exaggerated phenotype even in the absence of the inducer. The next

step was to find a middle ground and ensure the optimal expression of msfGFP-MinC which still showed some level of localisation and gave a strong enough signal to be visualised.

To achieve this middle ground, we expressed the inducible msfGFP-MinC system from a chromosomal locus in the genome via Tn7 mediated transposition in the wildtype cell and tried to regulate the expression of msfGFP-MinC by controlling the amount of inducer cyclohexanone added. This process was a challenge, because we had no information about the expression levels of endogenous MinC to serve as a starting point. Often times we ended up adding too much inducer, resulting in elongate green cells as seen in the transformed mutant. This is where the $\Delta minC$ mutant proved useful as it did not have an existing amount of MinC expressed in the cell. We expressed the Tn7 inducible msfGFP-MinC in the $\Delta minC$ mutant to understand what amount of inducer could be optimal and identified the amount of inducer that caused msfGFP-MinC to localise. The cells were long, but msfGFP-MinC was not spread homogeneously across the cell like in the transformed mutant, instead localised to the prospective poles of the cell (Fig. 18C). When the same amount of inducer was used in the wildtype Tn7 inducible msfGFP-MinC system, msfGFP-MinC was seen to be localised to one pole (Fig. 18B).

Even though all the mutants were grown in the presence of iron to prevent the production of pyoverdine, we need to be absolutely sure that the signal is from msfGFP-MinC. This can be done by fluorescent tagging MinC in a mutant unable to produce pyoverdine ($\Delta pvdS$) (Zhang and Rainey, 2013) or using antibody staining of the protein to check if the localisation at the cell pole can be solely attributed to that of msfGFP-MinC. Only further studies on the fluorescent tagged mutants can establish the nature of behaviour of MinC in *P. fluorescens*. At first look, it is indicative of an oscillatory system for ensuring cell division like in *E. coli* rather than the immobile system in *B. subtilis*, which would mean there would be MinC localisation at both the poles.

The primary objective of deleting *pbp1A* and *minC* and fluorescent tagging MinC was to understand their function in the context of the evolved $\Delta mreB$ mutants. This will help us understand the effect of the point mutation in *pbp1A* and how it would be improving

the fitness of $\Delta mreB$ mutants. Deleting MinC and replacing it with the described Tn7 inducible fluorescent tagged construct in the spherical $\Delta mreB$ mutants (both the ancestor and the evolved strain) then observing its localisation will provide insights on the involvement of MinC in symmetric division after evolution in the mutants. The $\Delta mreB$ mutants are very sick and extremely susceptible to any manipulations that might affect the cell integrity. Two step allelic exchange is a good method to introduce mutations, however the cycloserine enrichment step that selects the double crossover mutant is biased: wildtype revertants will likely outcompete unfit mutants during the long growth step required. An efficient way to select for deletion mutants, by reducing bias during counterselection would help isolate costly mutants. One option would be to use the SacB counterselection system instead of tetracycline resistance, which converts sucrose supplemented in the media to levans that are toxic to the cells. The counterselection is carried out in sucrose agar plates; streaking merodiploids to this plate results in single colonies of each double crossover type and unfit mutants do not compete against wildtype revertants (Huang and Wilks, 2017).

This study serves as a pilot investigation of the evolution of cell division and shape in *P. fluorescens*. Most results obtained in the study are preliminary and need more replicates and further analysis to be ascertained. Nonetheless, it has findings that can pave way to exciting new understanding of the evolution of cell shape. The study established a need for re-evaluation of understanding what the point mutation in *pbp1A* might actually be contributing to the evolved $\Delta mreB$ mutant and attempted to understand the function and dynamics of MinC in *P. fluorescens* SBW25. It has set up the possibility for a new long-term evolution experiment and Tn5 suppressor mutagenesis. Apart from the conceptual contributions of the study, we made huge improvements in the way the research group as a whole visualizes bacterial cells under the microscope. The use of membrane dye enabled the development of automated cell measurement programs, improving the accuracy of cell measurements substantially. The study exploited the use of automated cell segmentation and measurement programs, pointed out the possible weaknesses such programs could have and consequently led to the improvement of such issues. It has also sparked the development of efficient counter selection mechanisms for mutations or deletions that have a negative impact on the cell. In short, this study lays the foundation for detailed analysis of the compensatory mutations in the evolved $\Delta mreB$ mutants and the

function and interactions of MinC, improved cloning, microscopy and cell morphology measurement techniques.

MATERIALS AND METHODS:

Media and growth conditions

Pseudomonas fluorescens SBW25 and derived strains were grown either in 6mL of Lysogeny Broth (LB) (10 g/L Tryptone, 10 g/L NaCl, 5 g/L Yeast extract) or King's Medium B (KB) (1.5 g/L K₂HPO₄, 1.5 g/L MgSO₄·[7H₂O], 20 g/L Proteose Peptone No.3, 10 mL Glycerol) in 15mL universal bottles (microcosm) or 5mL of M9 minimal media supplemented with succinate (34 g/L Na₂HPO₄, 15 g/L KH₂PO₄, 2.5 g/L NaCl, 5.0 g/L NH₄Cl, 24.65 g/L MgSO₄, 14.7 g/L CaCl₂, 20mM Succinate) in 10mL capped test tubes at 28°C and *Escherichia coli* derived strains were grown in 5mL LB in 14mL capped test tubes with antibiotics and other supplements added when necessary. Depending on the experiment SOC, (Super Optimal media with Catabolite repression) (20 g/L Tryptone, 5 g/L Yeast extract, 10 mM NaCl, 25 mM KCl, 10 mM MgCl₂, 10 mM MgSO₄, 20mM Glucose) was also used occasionally. Liquid cultures were shaken at 220-250 rpm, unless otherwise mentioned. Whenever necessary, bacteria were grown in Petri dishes with 20mL of the above-mentioned media added, supplemented with 1.2 % agar. The bacterial stocks were frozen at -80°C in 20% Glycerol, with 2 parts of the culture added to 1 part of Glycerol.

Antibiotics and additional supplements

All antibiotics and supplement solutions were filter sterilised and used at the listed concentrations:

Antibiotic / Supplement	Concentration
Tetracycline (Tet)	12.5 µg/ml
Kanamycin (Kan)	100 µg/ml
Nitrofurantoin (NF)	100 µg/ml
Gentamycin (Gm)	100 µg/ml
Cycloserine (CS)	16 µg/ml

Ferrous ammonium sulphate (FeNH ₄ SO ₄)	16.7 mM
Cyclohexanone (Chn)	2%(v/v)

Table 1: Antibiotics and supplements used in this study

Bacterial strains

P. fluorescens strains

SBW25 (Rainey and Bailey, 1996) was the source strain for all *P. fluorescens* strains.

Annotation	Strain Name	Genotype/Description	Construction vector	Reference/Source
MPB13858	SBW25	Ancestral strain	-	(Rainey and Bailey, 1996)
MPB17743	<i>pbp1A</i> (G1450A)	PFLU0406 (G1450A)	-	(Yulo et al., 2018)
MPB17225	Δ <i>pbp1A</i>	Knockout of PFLU0406	MPB16739	This study
MPB17947	Red- <i>pbp1A</i> (G1450A)	PFLU0406 (G1450A), attTn7::Tn7-PntpII-mScarlet-I-Kan	MPB15801	This study
MPB18140	Green- <i>pbp1A</i> (G1450A)	PFLU0406 (G1450A), attTn7-PntpII-sGFP2-Kan	MPB15811	This study
MPB18141	Red- Δ <i>pbp1A</i>	Knockout of PFLU0406, attTn7::Tn7-PntpII-mScarlet-I-Gm	MPB15815	This study
MPB17945	Green- Δ <i>pbp1A</i>	Knockout of PFLU0406, attTn7::Tn7-PntpII-sGFP2-Kan	MPB15811	This study
MPB18251	Δ <i>minC</i>	Knockout of PFLU4369	MPB18055	This study
MPB18411	Red- Δ <i>minC</i>	Knockout of PFLU4369, attTn7::Tn7-PntpII-mScarlet-I-Kan	MPB15801	This study

MPB18412	Green- Δ <i>minC</i>	Knockout of PFLU4369, attTn7::Tn7-PntpII-sGFP-I-Kan	MPB15811	This study
MPB16556	<i>msfGFP-minC</i>	<i>msfGFP-minC</i>	MPB16267	This study
MPB17943	WT-Tn7 inducible <i>msfGFP-MinC</i>	attTn7::Tn7-chnB- <i>msfGFP-minC-Gm</i>	MPB17751	This study
MPB18270	Δ <i>minC</i> -Tn7 inducible <i>msfGFP-MinC</i>	Knockout of PFLU4369, attTn7::Tn7-chnB- <i>msfGFP-minC-Gm</i>	MPB17751	This study

Table 2: *P. fluorescens* strains used in this study

***E. coli* strains**

Strain Name	Genotype/Description	Source/Reference
DH5 α - λ pir	Chemically competent	(Macinga et al., 1995)
One Shot™ Top10	Chemically competent	Invitrogen™
One Shot™ PIR1	Chemically competent	Invitrogen™

Table 3: *E. coli* strains used in this study

Plasmids and Cloning Vectors

Annotation	Plasmid	Genotype/Description	Ab ^R	Source
MPB15426	pUIC3 mini-mScarlet	mScarlet tagged vector for two-step allelic exchange with pBR322 origin	Tet	David Rogers
MPB13966	pUIC3 mini- <i>msfGFP</i>	<i>msfGFP</i> tagged vector for two-step allelic exchange with R6K origin	Tet	David Rogers
MPB14779	pUIC3 mini- <i>msfGFP</i>	<i>msfGFP</i> tagged vector for two-step allelic exchange with pBR322 origin	Tet	David Rogers

MPB16739	<i>pbp1A</i> deletion vector	Assembled DWR096/097 product from MPB13966 with MV8/9 and MV10/11 products from SBW25 genomic DNA by NEB™ HiFi protocol	Tet	This study
MPB15801	Tn7 RFP vector	plasmid pMRE-pSC101ori-oriT-Tn7-AraC-Pbad-tnsABCD-PntpII-mScarlet-I	Gm	Addgene™
MPB15811	Tn7 GFP vector	plasmid pMRE-pSC101ori-oriT-Tn7-AraC-Pbad-tnsABCD-PntpII-sGFP2	Kan	Addgene™
MPB15815	Tn7 RFP vector	plasmid pMRE-pSC101ori-oriT-Tn7-AraC-Pbad-tnsABCD-PntpII-mScarlet-I	Kan	Addgene™
MPB18055	<i>minC</i> deletion vector	Assembled DWR096/097 product from MPB14779 with MV35/36 and MV37/38 products from SBW25 genomic DNA by NEB™ HiFi protocol	Tet	This study
MPB16267	Plasmid MPB15426 with <i>msfGFP-minC</i> gene	Assembled DWR096/097 product from MPB15426 with MV1/2 and MV5/6 products from SBW25 genomic DNA and MV3/4 product from MPB13966 by NEB™ HiFi protocol	Tet	This study
MPB16831/ 16872	Cyclohexanone inducible <i>msfGFP-MinC</i>	Assembled MV18/19 product from MPB14616 with MV20/21 from SBW25 genomic DNA by NEB™ HiFi protocol	Kan	This study
MPB17751	Tn7-inducible <i>msfGFP-MinC</i> vector	assembled DWR222/223 product from MPB13833 with DWR224/25 product from MPB16831 plasmid by NEB™ HiFi protocol	Gm	This study
MPB14245	pRK2013	Conjugation helper	Kan	Rainey Lab
MPB00266	pUX-BF13	Transposition Helper	Amp	Rainey Lab

Table 4: Plasmid vectors used in this study

List of selected primers

Primers were synthesized by Integrated DNA Technologies TM

Number	Sequence(5'-3')
DWR129	CAAAGACGATGGCACCTACAAAA
DWR162	ATGCCGTACAGCTATCTTGGTTCAGCGAACTTGCTGGTGGCGGTCAC
DWR163	CTTGCTCACCATCATGGTCGGCAAAAGCGGCTTG
DWR164	TTTGCCGACCATGATGGTGAGCAAGGGCGAGGCAG
DWR165	CTTGGTCTAGCGGTTTCGGTTTGGCTACCACCGCCACCGCTCTTGTACAGCTCGT CCATGCCG
DWR166	AGCCAAACCGAACCGCTAGACCAAG
DWR167	GTCAGTAGTCAGTTGATGTAGTGCTCAAGTCTTGCCGGTTTTCGCTGTG
DWR168	AACCGAACCGCTAGACCAAGA
DWR169	TCTTGGTCTAGCGGTTTCGGTT
DWR170	GGAACACCTCAAGCAGGCTCA
DWR171	TGAGCCTGCTTGAGGTGTTCC
DWR213	CACCAAAGCTTTCACCACCCAA
DWR214	CAGCATAACTGGACTGATTTTCAG
DWR222	TAGGAGCTTGCGGCCCGGAC
DWR223	TCGATACCGTCGACCTCGAACC
DWR224	TTCCGAGTCGACGGTATCGATCTAGGGCGGCGGATTTGTC
DWR225	GTCCGGGCCGCAAGCTCCTAGACCCCTGGATTCTACCAATAAAAAAC
MV1	ATGCCGTACAGCTATCTTGGTTCAGAGGCGGGCGAACTTGCTGGTG
MV2	GAATTCCCATGATCATGGTCGGCAAAAGCGGCTTG
MV3	TTGCCGACCATGATCATGGGAATTCATAAAGGTG
MV4	CTTGGTCTAGCGGTTTCGGTTTGGCTGCCACCTCCGCCGCTTTTGTAGAGTTCATC CATGC
MV5	AGCCAAACCGAACCGCTAGAC
MV6	GTCAGTAGTCAGTTGATGTAGTGCTCCGGTTTTCGCTGTGCTATCAG
MV7	GCGTTGTTGAAGAAATTCGGC
MV8	ATGCCGTACAGCTATCTTGGTTCAGATCAACGCCCTGGAAATCGCCG
MV9	AAATCCAAAAGCCAGGGCCATGCGAACACCACACA
MV10	TCGCATGGCCCTGGCTTTTGGATTTCCAGAGAAAAGA
MV11	GTCAGTAGTCAGTTGATGTAGTGCTCCATTGTGCACCATCGACTC
MV12	ACGGCCAGGGAATCGAGGTTGT
MV13	GCGAGGTGATGATCTTTGTCCGCT
MV14	GGTCAACAACGTAAGGGCT
MV15	TGGCCGTGTCATTGATGTCGA
MV16	AGCCCAGTACGTTGTTGACC
MV17	TCGACATCAATGACACGGCCA
MV18	CTTGGACTCCTGTTGATAGATC
MV19	TTTGTAGAGTTCATCCATGC
MV20	GCATGGATGAACTCTACAAAAGCGGCGGAGGTGGCAGCCAAACCGAACCGCTA GAC

MV21	TCTATCAACAGGAGTCCAAGTTAAAGACGGATGATGTTCAACACATC
MV22	GCGGCAACCGAGCGTTC
MV31	GCGTAACCTGGCAAAATCGGT
MV32	AGAGCCATATGACCCGAGTATTTCA
MV33	TTTGCCAGCAGTTGACCGC
MV34	GACCCAAGTACCGCCACCTA
MV35	ATGCCGTACAGCTATCTTGGTTCAGCACGAAGATACTTTGCTTGGCG
MV36	GCGGCAGTATCCGGGTCGGCAAAAGCGGCTTGT
MV37	CTTTTGCCGACCCGGATACTGCCGCATTTTCC
MV38	GTCAGTAGTCAGTTGATGTAGTGCTTTCCTTCACGTCTTCAACGC
MV39	ATAACTGTCTTGTGGCCGCG
MV40	CGCGGCCACAAGACAGTTAT
MV47	TTTTCGTACAACCTTGGCTTCA
MV48	GGTTGATACGCAGGCAGTCG
MV49	TCAAGAATGACTGGAACGCC
MV50	CGATGTTCCACGGTCTTGCCC

Table 5: Primers used in this study

Polymerase Chain Reaction

For cloning and verification of constructs, PCR was used. Polymerase mixes used included Phusion™ 2X master Mix, Q5™ 2X master mix for normal PCRs and TopTaq™ 2X master mix for Colony PCRs. Normal PCRs were done in a volume of 50µL, while Colony PCRs were done in a volume of 25µL in 200µL PCR reaction tubes. The template was obtained from genomic extraction, plasmid mini prep, or directly from cells. Large sized backbone plasmids MPB13966 and MPB15426 were digested prior to the reaction with 1uL of SpeI (NEB™) restriction enzyme at 37°C for 15 minutes and 80°C for 20 minutes for enzyme deactivation, to ensure efficient amplification. All obtained PCR products were purified using the QIAGEN QIAquick® PCR purification kit, following the instructions in the user's manual. For PCR products obtained from plasmid templates, an additional step of DpnI (NEB™) restriction enzyme digestion was included. 45uL of the amplicon was treated with 1µL of DpnI at 37°C for 1 hour, to remove the presence of undigested plasmid remains. The obtained products were visualised via gel electrophoresis on 1% molecular grade agarose gel with 0.01% SYBR Safe ® added.

Components	Volume
Template (10-100ng)	1.00µL
Forward and reverse primer(100µM)	1.25µL each
Polymerase Mix	25.00µL
Ultrapure ® Water	21.5µL
Total	50.00µL

Table 6: Components used for normal PCR

Process	Temperature	Duration	Cycle(s)
Denaturation	98°C	30 s	1
Denaturation	98°C	10 s	35
Annealing	60°C - 72°C	20 s	35
Extension	72°C	90 -180 s	35
Additional Extension	72°C	600 s	1

Table 7: Reaction conditions for normal PCR

Components	Volume/Concentration
Template	Touch of a colony from a plate/2µL of an overnight culture
Forward and reverse primer(100µM)	1.25µL each
Polymerase Mix	12.50µL
Ultrapure ® Water	10.00µL/8.00µL
Total	25.00µL

Table 8: Components used for colony PCR

Process	Temperature	Duration	Cycle(s)
Denaturation	94°C	30 s	1
Denaturation	94°C	10 s	35
Annealing	50°C - 60°C	20 s	35
Extension	72°C	90 -180 s	35
Additional Extension	72°C	600 s	1

Table 9: Reaction conditions for colony PCR

Enzymatic assembly of DNA fragments:

NEBuilder™ HiFi DNA Assembly Master Mix was used to assemble separately amplified DNA strands with overlapping sequences at the ends. The master mix has three components:

- Exonuclease: Chews away the 5' end of DNA, creating 3' overhangs. This results in the annealing of sequences, by virtue of complementarity of the overhangs.
- DNA polymerase: Fills in the base gaps in the annealed sequences.
- DNA ligase: Joins the adjacent sequences, by sealing the discontinuities.

The assembly components were added in the appropriate ratios and the reaction was carried out at 50°C for the suggested amount of duration as suggested by the user's manual.

Chemical Transformation of *E. coli*

Strains mentioned in Table () were used for chemical transformation. 50 µL of chemically competent cell culture contained in a 1.5 mL Eppendorf® tube was thawed on ice, to which 2 µL of the chilled Gibson assembled product was added. The tube was kept on ice for 30 minutes, followed by a heat shock at 42°C in a water bath for 30 seconds. The tube was immediately transferred to ice for 2 minutes and 350 µL of pre-warmed SOC media was added. This was then incubated at 37°C for an hour at 700 rpm on a shaking Thermomixer®. The cells were then plated on LB plates with tetracycline at 10⁰ and 10⁻¹ dilution. Since the vector always had a fluorescent marker, isolated fluorescent colonies on the plates were selected for further screening by colony PCR. Plasmid DNA from PCR positive colonies was extracted using the QIAGEN® Mini prep kit following the instructions on the user's manual.

Electroporation of *P. fluorescens*

All Tn7 constructs were made by electroporation. 1 ml of an O/N culture of SBW25 in an Eppendorf® tube was centrifuged at 13000 rpm for 1 minute and the supernatant was discarded. The pellet was resuspended in 1 ml of ice-cold 10% glycerol, 1mM HEPES [2-(4-hydroxyethyl)piperazin-1-yl]ethanesulfonic acid] solution and centrifuged at 13000 rpm at 4°C and the supernatant was discarded. This step was repeated 2 more times, following which the pellet was resuspended in 50 µL of ice-

cold 10% glycerol, 1mM HEPES solution and placed on ice. To these electrocompetent cells, 5 μ L of chilled Gibson assembled product (100-200 ng) was added. For Tn-7 inducible *msfGFP*-*MinC* vector, transposition helper pUXBF13 was also added such that the total volume of the products did not exceed 5 μ L. Electroporation was done with a BIO-RAD MicroPulser™ using the Ec1 (1.8kV) setting on cells transferred to pre-chilled 0.1cm electroporation cuvettes. 1 ml of pre-warmed SOC was added to the cells immediately after, transferred to a 1.5 ml Eppendorf® tube and incubated at 28°C in a shaking incubator at 220 rpm. 50 μ L of the incubated cells were then plated on LB + selection at 10^0 and 10^{-1} dilution.

Two- step allelic replacement by homologous recombination

Two step allelic exchange was used to obtain deletion and insertion mutants (Fig. 19) (Hmelo et al., 2015). In the case of *pbp1A* and *minC* deletion, the vectors used for this method were designed in such a way that the pUIC3 backbone contained 800 bp long DNA fragments flanking the gene of interest. In the case of insertion of *msfGFP* in the 5' end of *minC* gene, the vectors were designed such that the pUIC3 backbone contained the 800bp upstream region of *minC* including the start codon, *msfGFP* and 800bp sequence of *minC* after the start codon. All pUIC3 originated vectors have tetracycline resistance and a fluorescence marker. The first step is to insert the vector in to *P. fluorescens* SBW25. Once the plasmid is inserted, it leads to the first recombination event. This could in the upstream or downstream region of the gene, resulting in the insertion of the whole plasmid in to the gene, giving rise to a merodiploid which will have tetracycline resistance and the fluorescence marker (1XO mutant). The plasmid by itself is unable to replicate in the cell because the origin of replication in the vector (R6K or pBR332) is functional only in some strains of *E. coli*. The step is done by conjugation as described below.

a) Triparental conjugation (Primary Crossover event)

To transfer the desired vector to *P. fluorescens* SBW25, triparental conjugation was used. The strains used for the conjugation include

- Recipient strain: SBW25 WT or derived strains
- Donor strain: *E. coli* vector
- Helper strain: pRK2013

Overnight(O/N) cultures of the above strains were grown in appropriate selection. 500µL of the recipient strain O/N culture was heat shocked at 45°C in a Thermomixer®. 500µL each of the donor and helper strain O/N culture was mixed in a 1.5mL Eppendorf® tube and centrifuged at 13000 rpm for 1 minute in an Eppendorf® centrifuge. The supernatant was discarded and the pellet was resuspended in 500µL LB, to which 500µL of the heat shocked recipient was added. The mixture was centrifuged at 13000 rpm for 1 minute and supernatant was removed. The pellet was resuspended in 100 µL of LB and the whole volume was pipetted carefully on to the centre of a LB plate and carefully spread in to a 2 cm radius circle using a fresh pipette tip to form a mating patch. The plate was then kept for incubation at 28°C for 24 hours in the upright position, following which the mating patch was carefully scraped off and resuspended in 1 mL of LB and vortexed. 100 µL of a 10⁰ and 10⁻¹ dilution of this mixture was plated on to LB, with nitrofurantoin and tetracycline added to selectively prevent the growth of *E. coli* and only allow the growth of the merodiploid respectively. The plate was then incubated at 28°C for 48 hours.

Once the merodiploid is obtained, next step is to facilitate the selection of cells that have undergone the second recombination event between the cloned DNA fragment and the chromosome, which is a rare event. The second recombination can either result in an insertion/deletion or reversion to WT. A large volume of media is inoculated with a very low volume of cells, to increase the number of replications that can happen and consequently the chance of the second recombination event. Following this, a small volume of these cells is transferred to fresh media. These cells are grown in the absence of tetracycline for a short while, to allow the few cells that have undergone second cross over (2XO mutants) to increase in number. Tetracycline is then added, which inhibits the growth of the 2XO mutants. The addition of cycloserine after this, results in the death of growing cells (1XO mutants), effectively increasing the chances of acquiring a 2XO mutant from the mixture. The method is described below:

b) Cycloserine enrichment (Secondary crossover event)

Since the vectors had tetracycline resistance and a fluorescent marker, the primary recombinant will be fluorescent and resistant to tetracycline. 6-8 antibiotic resistant fluorescent colonies were picked from the final plates obtained after conjugation to make a mixed O/N culture. 20 μL of this O/N culture was added to pre-sterilised 400mL of LB in a 1L Erlenmeyer® flask and grown in a shaking incubator at 28°C at 160 rpm for 24 hours. Next day, 400 μL of the 24-hour grown culture was added to pre-sterilised 20 mL of LB in a 250 mL Erlenmeyer® flask and grown in a shaking incubator at 28°C at 220 rpm for 30 minutes. After 30 minutes, 20 μL of tetracycline was added to the flask and the culture was put back in the incubator and grown for another 2 hours. After this, 1 mL of cycloserine was added to the culture and put back in the incubator to grow for an additional 5 hours. After the 5-hour period, 50 μL of 10^0 , 10^{-1} and 10^{-2} dilutions of the culture were plated on LB plates supplemented with iron and incubated at 28°C for 48 hours.

Non-fluorescent colonies obtained on plates tested positive using colony PCR were selected for further screening.

Illumina Sequencing and Mutation detection

Genomic DNA was extracted by the QIAGEN DNeasy® Tissue and Blood kit following instructions in the user's manual and sequenced by the Max Planck Institute's sequencing service using the Illumina MiSeq Next generation sequencing system. 1,929,782 reads were obtained, trimmed using BBDuk plugin and aligned to reference genome of *P. fluorescens* SBW25 (AM181176.4). The average length of the reads was 146.9 ± 14.8 bp, with the longest read being 151 bp long and shortest read being 35 bp. The aligned sequence was then analysed to check for the presence of single nucleotide polymorphisms/variations. The minimum number of reads required to define a base pair as a variation was set as 10 and only variants that appeared in 95% of the reads at the site in question were counted.

Sanger Sequencing

5 μL of PCR products to be sequenced was treated with 2 μL of EXOSAP-IT™ at 37°C for 15 minutes and 80°C for 15 minutes. For the sequencing reaction, 1 μL of the

purified mix was used. The reaction was carried out in Applied biosystems™ 96 well plates (100 µL), with each well assigned to a specific primer and the amplicon to be sequenced. The reaction mix composition and reaction conditions are mentioned in Table 10 and 11. After the reaction, 50 µL of properly mixed Big Dye Xterminator™ (BDX) components was added per reaction to remove labels that were not incorporated. The BDX mix for a single reaction contains 37 µL of SAM™ solution and 13 µL of Xterminator™ solution. Following this the reaction plate was shaken for 30 minutes in a plate shaker and centrifuged at 1000 rpm for 2 minutes. This was then submitted to Max Planck Institute's sequencing facility.

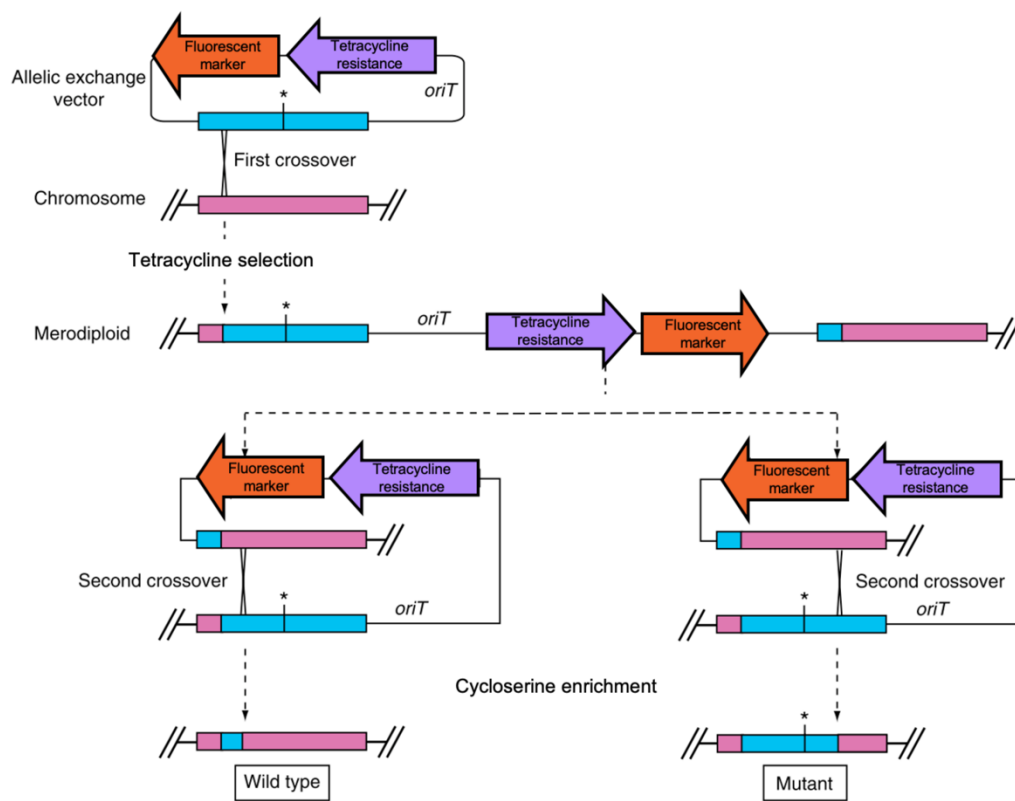


Fig. 19: Two step allelic exchange. The merodiploid resulting from the first crossover is selected by tetracycline resistance and presence of the fluorescence marker. This merodiploid undergoes a second crossover event, which gives rise to the mutant or wildtype revertant. Because this event is very rare, a slow growth regime in the presence of cycloserine is used to enrich for double mutants. Image adapted from Hmelo et al., 2015 and modified for the purpose of this study.

Components	Volume
Template (10-100ng)	1.00 μ L
Primer(100 μ M)	1.00 μ L
Big Dye	0.50 μ L
5X Big Dye buffer	2.00 μ L
Ultrapure $\text{\textcircled{R}}$ Water	5.50 μ L
Total	10.00 μ L

Table 10: Components used for Sanger sequencing

Process	Temperature	Duration	Cycle(s)
Denaturation	96 $^{\circ}$ C	60 s	1
Denaturation	96 $^{\circ}$ C	10 s	30
Annealing	56 $^{\circ}$ C	15 s	30
Extension	60 $^{\circ}$ C	240 s	30

Table 11: Reaction conditions used for Sanger sequencing

Fluorescence fitness Assay

All the strains to be competed against each other where grown in 6mL KB microcosms for 24 hours to reach stationary phase. The strains had a green or red fluorescent marker inserted in the *glmS* gene of SBW25 via Tn7 mediated transposition. 200 ml of each O/N culture of the strains to be competed against each other (with different fluorescent markers) were added to a 1.5 ml Eppendorf $\text{\textcircled{R}}$ tube and vortexed well. 60 μ L of this mixture was then used to inoculate a fresh 6mL KB microcosm and allowed to grow for 24 hours to reach stationary phase (T_0 culture). Next day, 10 μ L of the culture was serially diluted to 10^{-4} in 1 mL PBS and the cells in the T_0 culture were counted using MACSQuant TM Flow cytometer. Due to the presence of red and green fluorescent tags in the competing strains, the flow cytometer can give separate counts for each strain. 60 μ L of the T_0 culture was added to a fresh 6mL KB microcosm (1:100 dilution) and allowed to grow for 24 hours to reach stationary phase (T_1 culture). Next day, 10 μ L of the T_1 culture was diluted to 10^{-4} in 1 mL PBS and the cells were counted using MACSQuant TM Flow cytometer. The Malthusian equation for calculating fitness of a population is (Lenski et al., 1991) :

$$r = \frac{\ln\left(\frac{N_t}{N_0}\right)}{t}$$

Where r is the Malthusian parameter, t is the time between the initial and final time point, N_0 is the number of individuals at the initial time point, N_t is the number of individuals at final time point and \ln is the natural logarithm. In this study, frequency of cells (f), rather than the absolute counts were used for relative fitness calculations, due to the limitations of the flow cytometer. For strains A and B competing against each other, frequency of cells of strain A at timepoint n (T_n) is expressed as:

$$f_{T_n}^A = \frac{N_{T_n}^A}{N_{T_n}^A + N_{T_n}^B}$$

Fitness of strain A relative to strain B was calculated from timepoints T_0 and T_1 as:

$$\frac{r^A}{r^B} = \frac{\ln\left(\frac{f_{T_1}^A}{0.01f_{T_0}^A}\right)}{\ln\left(\frac{f_{T_1}^B}{0.01f_{T_0}^B}\right)}$$

Where 0.01 is the dilution factor, r^A and r^B are the Malthusian parameters of strain A and B respectively.

Inducer Assay

To assess the right amount of inducer required to visualize msfGFP-MinC, the WT and $\Delta minC$ Tn7 cyclohexanone inducible msfGFP-MinC, wildtype and $\Delta minC$ strains were inoculated from glycerol stocks in 6mL LB microcosms and grown for 16-18 hours. 60 μ L of this was used to inoculate fresh 6 mL LB microcosms supplemented with different amounts of 2% cyclohexanone solution and without it to serve as a control. The amount of cyclohexanone added ranged from 0.001 μ L to 20 μ L. This included 0.001, 0.01, 0.1, 1, 2.5, 5, 10 and 20 μ L. The amount of cyclohexanone that gave the most optimal expression of msfGFP i.e. no long cells and localised green signals was found to be 0.01 μ L and chosen as the appropriate inducer amount.

Microscopy

Strains to be visualised were inoculated in LB or M9 minimal media as per need from glycerol stocks and grown for 16-18 hours. For the cyclohexanone inducible mutants,

0.01 μL of 2% cyclohexanone solution was added to the microcosms. If required, 6 μL of Ferrous ammonium sulphate (FeNH_4SO_4) was added. 1.0 – 1.5 μL of the O/N culture were then planted on a gel pad (2% low EEO agarose in M9 minimal media supplemented with succinate). For membrane staining, 1 μL of 1 $\mu\text{g}/\text{ml}$ solution of FMTM4-64 (Thermofisher®) was used. A glass coverslip over double-sided tape was used to seal the sample. Bacteria were visualized and images were captured on an Axio Imager 2 microscope from Carl ZeissTM using a 63X/NA 1.4 oil immersion objective lens. 385 nm, 475 nm and 555 nm wavelength lasers were used to visualise DAPI, GFP and FMTM4-64 signals respectively. All membrane-stained images were deconvoluted using Carl ZeissTM image processing software using the default settings to minimise background noise.

Cell measurements

Deconvoluted membrane stained cell images were used for cell measurements. The measurements of *pbp1A* mutants and corresponding wildtype cells were carried out using the cell segmentation program developed by Tatyana Pichugina (Fig. 20). Watershed segmentation was used to identify the contour of each cell and a rectangle was fitted around each cell. The major and minor axis of the rectangle was considered the length and width of the cell respectively. Area was calculated by counting all the pixels enclosed by the contour. The program had difficulty identifying dividing and clumped cells as separate objects. Such objects were excluded from the measurements.

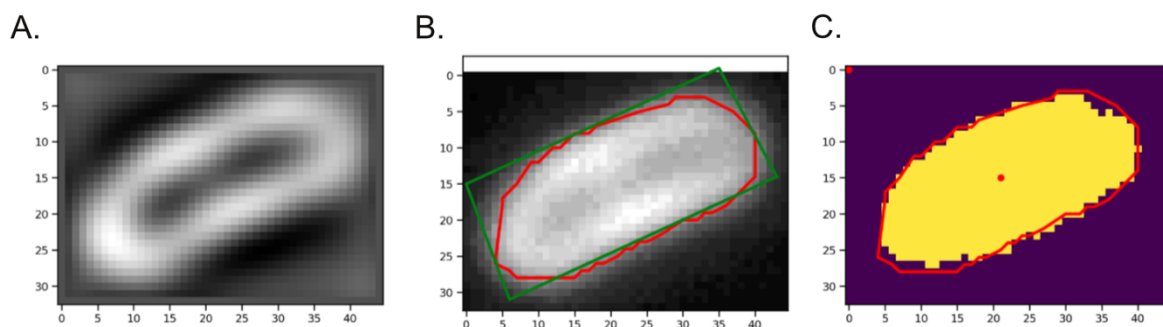


Fig. 20: Workflow of *pbp1A* related cell measurements. A) A cell to be processed is identified as an object by the program. B) The contour of the cell is extracted by watershed segmentation. The rectangle drawn around the cell defines the length and width of the cell. C) The number of pixels enclosed by the contour was used to define the area of the cell.

The previous program cannot be used to provide accurate measurements for long cells that has the tendency to curl. Hence, for the $\Delta minC$ cells and control wildtype cells, cell contour data was extracted using the semi-automated JFilament plugin of ImageJ. The plugin extracts the co-ordinate data of each pixel that constitutes the cell contour as a data file (Smith et al., 2010). This data file was then analysed by a Mathematica program designed by Nikola Ojkic as described in (Ojkic et al., 2016) to extract the length and width of the cells (Fig. 21).

Statistical Analysis

All data were log transformed for the analysis. Analysis of Variance (ANOVA) was performed using the Fit Model module of JMP 7 (SAS). All predictors were treated as fixed factors and higher order interactions were ignored unless otherwise specified. Mean and standard error of all data were calculated and plotted using GraphPad Prism 8 software.

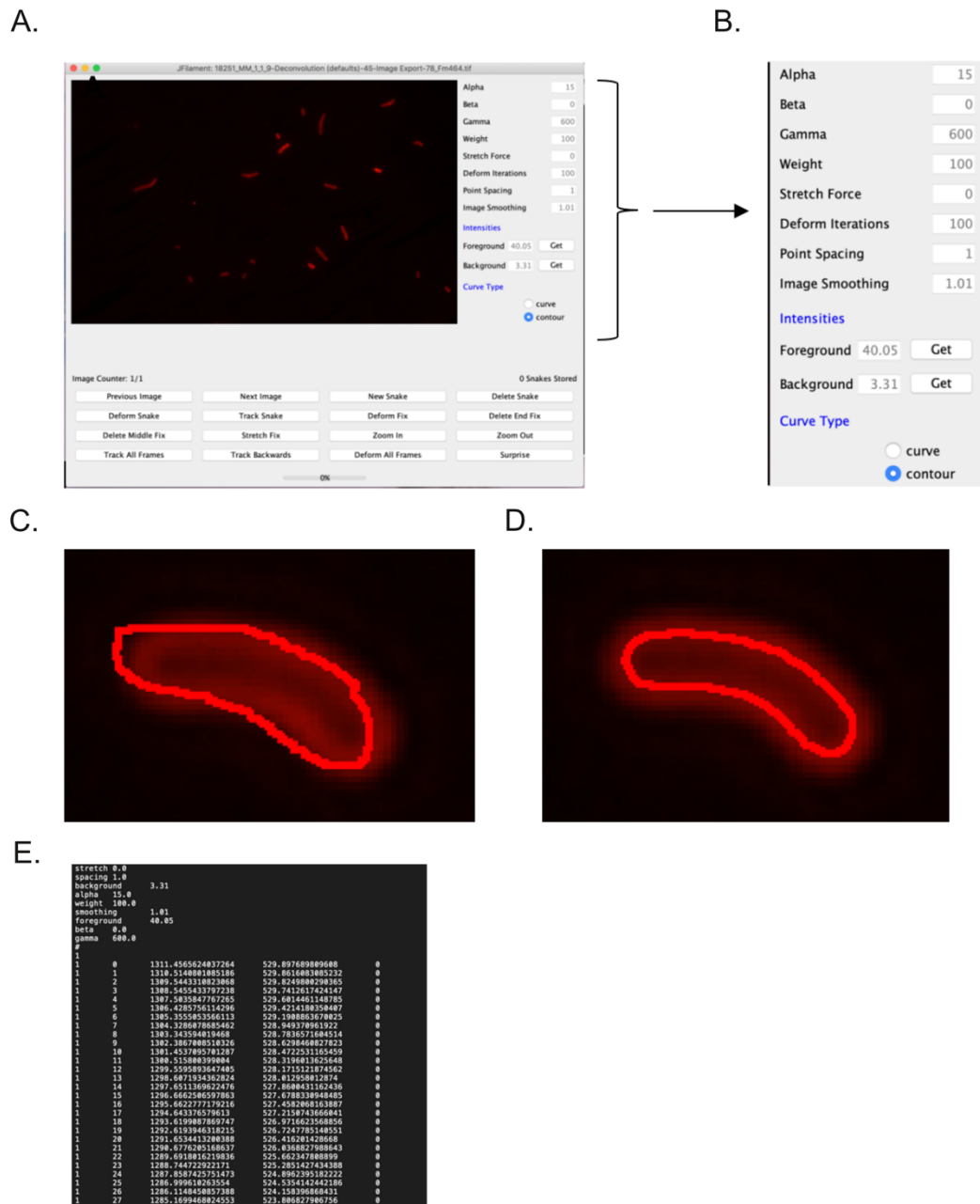


Fig. 21: Workflow for $\Delta minC$ mutant measurements. A) User console of Jfilament2D in ImageJ with the picture to be processed. B) Settings used for measurements in this study, foreground and background intensity was obtained by clicking the background and an object in the foreground respectively C) Outline drawn by the user on a zoomed in cell. D) Outline is processed by the program, to give a fitted contour. E) The fitted contours of each cell are saved as a data file, that lists coordinate positions of each pixel in the contour. This data is then analysed to give cell morphology parameters.

REFERENCES

- Bhuvanachandra, B., Madhuprakash, J., and Podile, A.R. (2018). Active-site mutations improved the transglycosylation activity of *Stenotrophomonas maltophilia* chitinase A. *Biochim. Biophys. Acta - Proteins Proteomics* 1866, 407–414.
- de Boer, P.A., Crossley, R.E., Hand, A.R., and Rothfield, L.I. (1991). The MinD protein is a membrane ATPase required for the correct placement of the Escherichia coli division site. *EMBO J.* 10, 4371–4380.
- de Boer, P.A.J., Crossley, R.E., and Rothfield, L.I. (1989). A division inhibitor and a topological specificity factor coded for by the minicell locus determine proper placement of the division septum in *Escherichia. coli*. *Cell* 56, 641–649.
- Carter, T., Buensuceso, R.N.C., Tammam, S., Lamers, R.P., Harvey, H., Howell, P.L., and Burrows, L.L. (2017). The type IVa pilus machinery is recruited to sites of future cell division. *MBio* 8, 1–18.
- Cho, H., Wivagg, C.N., Kapoor, M., Barry, Z., Rohs, P.D.A., Suh, H., Marto, J.A., Garner, E.C., and Bernhardt, T.G. (2016). Bacterial cell wall biogenesis is mediated by SEDS and PBP polymerase families functioning semi-Autonomously. *Nat. Microbiol.* 1, 1–21.
- Fellay, R., Krisch, H.M., Prentki, P., and Frey, J. (1989). Omegon-Km: a transposable element designed for in vivo insertional mutagenesis and cloning of genes in Gram-negative bacteria. *Gene* 76, 215–226.
- Flores, S.A., Howell, M., Daniel, J.J., Piccolo, R., and Brown, P.J.B. (2018). Absence of the Min system does not cause major cell division defects in *Agrobacterium tumefaciens*. *Front. Microbiol.* 9, 1–14.
- Hmelo, L.R., Borlee, B.R., Almblad, H., Love, M.E., Randall, T.E., Tseng, B.S., Lin, C., Irie, Y., Storek, K.M., Yang, J.J., et al. (2015). Precision-engineering the *Pseudomonas aeruginosa* genome with two-step allelic exchange. *Nat. Protoc.* 10,

1820–1841.

Huang, W., and Wilks, A. (2017). A rapid seamless method for gene knockout in *Pseudomonas aeruginosa*. *BMC Microbiol.* *17*, 1–8.

Job, V., Carapito, R., Vernet, T., Dessen, A., and Zapun, A. (2008). Common alterations in PBP1a from resistant *Streptococcus pneumoniae* decrease its reactivity toward β -lactams: Structural insights. *J. Biol. Chem.* *283*, 4886–4894.

Lenski, R.E. (2017). Experimental evolution and the dynamics of adaptation and genome evolution in microbial populations. *ISME J.* *11*, 2181–2194.

Lenski, R.E., Rose, M.R., Simpson, S.C., and Tadler, S.C. (1991). Long-term experimental evolution in *Escherichia coli*. *I. Adaptation and divergence during 2000 generations.* *Am. Nat.* *138*, 1315–1341.

Levin, P.A., Shim, J.J., and Grossman, A.D. (1998). Effect of minCD on FtsZ ring position and polar septation in *Bacillus subtilis*. *J. Bacteriol.* *180*, 6048–6051.

Li, Z., Nimtz, M., and Rinas, U. (2014). The metabolic potential of *Escherichia coli* BL21 in defined and rich medium. *Microb. Cell Fact.* *13*, 1–17.

Lutkenhaus, J. (2007). Assembly Dynamics of the Bacterial MinCDE System and Spatial Regulation of the Z Ring. *Annu. Rev. Biochem.* *76*, 539–562.

Macinga, D.R., Parojcic, M.M., and Rather, P.N. (1995). Identification and analysis of aarP, a transcriptional activator of the 2'-N-acetyltransferase in *Providencia stuartii*. *J. Bacteriol.* *177*, 3407–3413.

Monahan, L.G., Turnbull, L., Osvath, S.R., Birch, D., Charles, I.G., and Whitchurch, C.B. (2014). Rapid conversion of *Pseudomonas aeruginosa* to a spherical cell morphotype facilitates tolerance to carbapenems and penicillins but increases susceptibility to antimicrobial peptides. *Antimicrob. Agents Chemother.* *58*, 1956–1962.

Moon, C.D., Zhang, X.X., Matthijs, S., Schäfer, M., Budzikiewicz, H., and Rainey, P.B. (2008). Genomic, genetic and structural analysis of pyoverdine-mediated iron acquisition in the plant growth-promoting bacterium *Pseudomonas fluorescens* SBW25. *BMC Microbiol.* 8, 1–13.

Ogura, T., Bouloc, P., Niki, H., D'Ari, R., Hiraga, S., and Jaffe, A. (1989). Penicillin-binding protein 2 is essential in wild-type *Escherichia coli* but not in *lov* or *cya* mutants. *J. Bacteriol.* 171, 3025–3030.

Ojkic, N., López-Garrido, J., Pogliano, K., and Endres, R.G. (2016). Cell-wall remodeling drives engulfment during *Bacillus subtilis* sporulation. *Elife* 5, 1–30.

Pinho, M.G., Kjos, M., and Veening, J.W. (2013). How to get (a)round: Mechanisms controlling growth and division of coccoid bacteria. *Nat. Rev. Microbiol.* 11, 601–614.

Poulsen, B.E., Yang, R., Clatworthy, A.E., White, T., Osmulski, S.J., Li, L., Penaranda, C., Lander, E.S., Shoresh, N., and Hung, D.T. (2019). Defining the core essential genome of *Pseudomonas aeruginosa*. *Proc. Natl. Acad. Sci. U. S. A.* 116, 10072–10080.

Price, M.N., Wetmore, K.M., Waters, R.J., Callaghan, M., Ray, J., Liu, H., Kuehl, J. V., Melnyk, R.A., Lamson, J.S., Suh, Y., et al. (2018). Mutant phenotypes for thousands of bacterial genes of unknown function. *Nature* 557, 503–509.

Rainey, P.B., and Bailey, M.J. (1996). Physical and genetic map of the *Pseudomonas fluorescens* SBW25 chromosome. *Mol. Microbiol.* 19(3), 521–533.

Ramirez-Arcos, S., Szeto, J., Beveridge, T.J., Victor, C., Francis, F., and Dillon, J.A.R. (2001). Deletion of the cell-division inhibitor MinC results in lysis of *Neisseria gonorrhoeae*. *Microbiology* 147, 225–237.

Rignall, T.R., Baker, J.O., McCarter, S.L., Adney, W.S., Vinzant, T.B., Decker, S.R., and Himmel, M.E. (2002). Effect of single active-site cleft mutation on product specificity in a thermostable bacterial cellulase. *Appl. Biochem. Biotechnol. - Part A*

Enzym. Eng. Biotechnol. 98–100, 383–394.

Rodrigues, C.D.A., and Harry, E.J. (2012). The min system and nucleoid occlusion are not required for identifying the division site in *Bacillus subtilis* but ensure its efficient utilization. PLoS Genet. 8.

Shiomi, D., Sakai, M., and Niki, H. (2008). Determination of bacterial rod shape by a novel cytoskeletal membrane protein. EMBO J. 27, 3081–3091.

Smith, M.B., Li, H., Shen, T., Huang, X., Yusuf, E., and Vavylonis, D. (2010). Segmentation and tracking of cytoskeletal filaments using open active contours. Cytoskeleton 67, 693–705.

van Teeffelen, S., and Renner, L.D. (2018). Recent advances in understanding how rod-like bacteria stably maintain their cell shapes. F1000Research 7, 241.

Veiga, H., and Pinho, M.G. (2012). Bacterial cell division : what it takes to divide a prokaryotic cell. CanalBQ 9, 18–26.

Veyrier, F.J., Biais, N., Morales, P., Belkacem, N., Guilhen, C., Ranjeva, S., Sismeiro, O., Péhau-Arnaudet, G., Rocha, E.P., Werts, C., et al. (2015). Common cell shape evolution of two nasopharyngeal pathogens. PLoS Genet. 11, 1–23.

Wachi, M., Doi, M., Tamaki, S., Park, W., Nakajima-Iijima, S., and Matsushashi, M. (1987). Mutant isolation and molecular cloning of mre genes, which determine cell shape, sensitivity to mecillinam, and amount of penicillin-binding proteins in *Escherichia coli*. J. Bacteriol. 169, 4935–4940.

Watve, M. (1997). Why rods and cocci. Resonance 2, 79–81.

Young, K.D. (2006). The Selective Value of Bacterial Shape. Microbiol. Mol. Biol. Rev. 70, 660–703.

Yulo, P.R., Desprat, N., Gerth, M.L., Liu, Y., Zhang, X.-X., Rainey, P.B., and

Hendrickson, H.L. (2018). Experimental evolution of cell shape in bacteria. BioRxiv
<https://doi.org/10.1101/263681>.

Zhang, X.X., and Rainey, P.B. (2013). Exploring the sociobiology of pyoverdinin-producing *Pseudomonas*. *Evolution* (N. Y). 67, 3161–3174.